Cell Reports

Compartmentalized control of Cdk1 drives mitotic spindle assembly

Graphical abstract

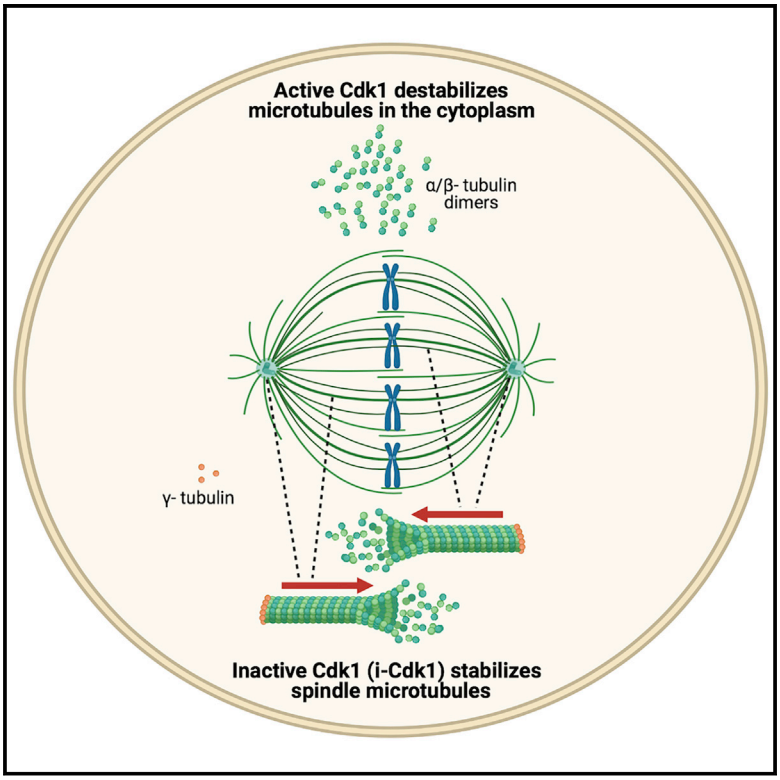

Authors

Angela Flavia Serpico, Francesco Febbraro, Caterina Pisauro, Domenico Grieco

Correspondence

domenico.grieco@unina.it

In brief

By cell fractionation, imaging, and genetic knockdown experiments in human cells, Serpico et al. find that a small fraction of Cdk1, the major M-phase promoting kinase, remains inhibited by phosphorylation in mitosis (i-Cdk1). i-Cdk1 is selectively localized at the mitotic spindle and necessary for its formation.

Highlights

- A small fraction of Cdk1 is inhibited by phosphorylation in mitosis (i-Cdk1)
- i-Cdk1 selectively localizes at the mitotic spindle and drives its formation
- i-Cdk1 controls PP1 and microtubule-stabilizing MAPs to promote spindle assembly

Serpico et al., 2022, Cell Reports *38*, 110305
January 25, 2022
https://doi.org/10.1016/j.celrep.2022.110305

CellPress

Cell Reports

CellPress
OPEN ACCESS

Report

Compartmentalized control of Cdk1 drives mitotic spindle assembly

Angela Flavia Serpico,[1,2] Francesco Febbraro,[1,2] Caterina Pisauro,[1,2] and Domenico Grieco[1,3,4,*]
[1]CEINGE Biotecnologie Avanzate, Naples, Italy
[2]DMMBM, University of Naples "Federico II", Naples, Italy
[3]Department of Pharmacy, University of Naples "Federico II", Naples, Italy
[4]Lead contact
*Correspondence: domenico.grieco@unina.it
https://doi.org/10.1016/j.celrep.2022.110305

SUMMARY

During cell division, dramatic microtubular rearrangements driven by cyclin B-cdk1 (Cdk1) kinase activity mark the onset of mitosis leading to dismantling of the interphase microtubular cytoskeleton and assembly of the mitotic spindle. During interphase, Cdk1 accumulates in an inactive state, phosphorylated at inhibitory sites by Wee1/Myt1 kinases. At mitosis onset, Cdc25 phosphatase dephosphorylates and activates Cdk1. Once activated, Cdk1 clears cytoplasmic microtubules by inhibiting microtubule-stabilizing and growth-promoting microtubule-associated proteins (MAPs). Nevertheless, some of these MAPs are required for spindle microtubule growth and spindle assembly, creating quite a conundrum. We show here that a Cdk1 fraction bound to spindle structures escapes Cdc25 action and remains inhibited by phosphorylation (i-Cdk1) in mitotic human cells. Loss or restoration of i-Cdk1 inhibits or promotes spindle assembly, respectively. Furthermore, polymerizing spindle microtubules foster i-Cdk1 aggregating with Wee1 and excluding Cdc25. Our data reveal that spindle assembly relies on compartmentalized control of Cdk1 activity.

INTRODUCTION

To prevent chromosome damage during spindle assembly, the microtubular interphase cytoskeleton must be dismantled at the onset of mitosis and, as many mitotic features, this is an event downstream cyclin B-cdk1 (Cdk1) activation. Indeed, Cdk1 activity clears cytoplasmic microtubules by directly or indirectly affecting several microtubule-stabilizing and -destabilizing microtubule-associated proteins (MAPs), inhibiting, for instance, the microtubule growth-promoting properties of ch-Tog and Map4 (Verde et al., 1990; Lieuvin et al., 1994; Mchedlishvili et al., 2018; Chang et al., 2001; Vasquez et al., 1999). Nevertheless, a number of these MAPs are required for spindle microtubule growth (Lieuvin et al., 1994; Ookata et al., 1995; Gergely et al., 2003). Thus, how the spindle assembles despite the potent microtubule-destabilizing action of Cdk1 is unknown. During interphase, Cdk1 accumulates in an inactive state, phosphorylated at inhibitory sites by Wee1/Myt1 kinases (Hunt, 2013). At mitosis onset, initial reversal of these phosphorylations by Cdc25 phosphatase is rapidly followed by full Cdk1 activation via positive feedback loops in which Cdk1 inhibits Wee1/Myt1 and stimulates Cdc25 (Hunt, 2013). Thus, inhibitory phosphorylation of Cdk1 has a crucial role in ensuring completion of interphase tasks before mitosis onset, but once Cdk1 activation begins, this control appears to be rapidly suppressed by autoactivatory feedback loops. Cdk1 is believed to be only inactivated upon spindle assembly by cyclin B degradation (Hunt, 2013). Nevertheless, early evidence indicated that cells expressing a Cdk1 version non-phosphorylatable at the inhibitory sites threonine 14 and tyrosine 15 (cdk1AF) rapidly entered mitosis but failed to assemble spindles (Krek and Nigg, 1991). These mitotic defects were, however, ascribed to premature mitosis onset in the presence of incompletely replicated DNA and not as a requirement for inhibitory phosphorylation of Cdk1 in spindle assembly (Krek and Nigg, 1991). In addition, evidence that an inhibited form of Cdk1 is present in meiotic and mitotic extracts from *Xenopus* eggs and mouse eggs was later reported (D'Angiolella et al., 2007; Oh et al., 2011). Here we examined if and how inhibitory phosphorylation of Cdk1 had a role for spindle assembly.

RESULTS

Dependence of spindle formation on inhibitory phosphorylation of Cdk1

To this end, we began analyzing spindle assembly upon downregulation of Wee1 expression by small interfering RNAs (siRNAs) in hTERT-RPE1 cells. To prevent premature mitosis onset upon Wee1 downregulation, 6 h post Wee1-siRNA treatment, cells were incubated with the selective and reversible Cdk1 inhibitor RO-3306 at 9 μM (high-RO) for a further 16 h, to allow completion of DNA replication and arrest cell cycle at G2 (Vassilev et al., 2006). As a control, part of the Wee1-siRNA-treated cells were previously complemented with a siRNA-resistant Wee1 expression vector (Visconti et al., 2015; Figures 1A and S1). Upon release from G2-arrest into fresh medium, containing the

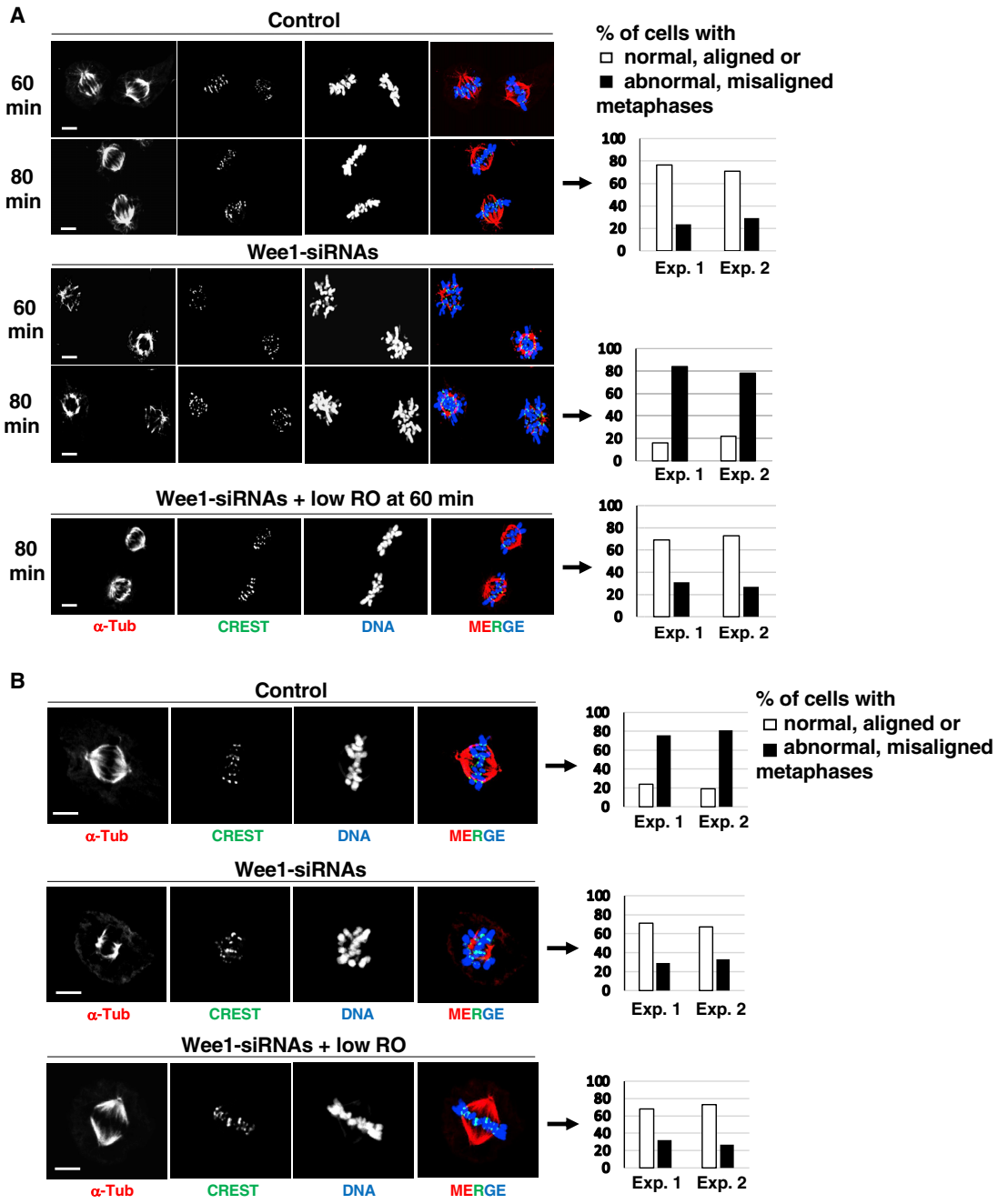

Figure 1. Wee1 downregulation affects spindle assembly

(A) hTERT-RPE1 cells were arrested at G2 by high-RO treatment, released, and fixed at 60 and 80 min of incubation in M/C medium (see STAR Methods). Control: Wee1-siRNA-treated cells previously transfected with siRNA-resistant Wee1 expression vector; Wee1-siRNAs: Wee1-siRNA-treated cells previously transfected with empty vector; Wee1-siRNAs + low-RO: Wee1-siRNAs to which low-RO was added by 60 min from G2-arrest release.

(B) hTERT-RPE1 cells were arrested at prometaphase with nocodazole, released, and fixed after 80 min of incubation in M/C medium. Control: cells treated with non-targeting siRNAs; Wee1-siRNAs: just Wee1-siRNA-treated cells; Wee1-siRNAs + low-RO: Wee1-siRNA-treated cells to which low-RO was added by 60 min from prometaphase-arrest release. Cells were fixed and stained for CREST (centromere marker, green), α-tubulin (α-Tub, red) and DNA (blue). Addition of vehicle (DMSO) had no effect on spindle assembly in Wee1-siRNA-treated cells. Graphs: y axis = percent of cells containing normal aligned (white bar) or abnormal misaligned (black bar) spindles at 80 min incubation; x axis = data from two independent experiments (Exp. 1; Exp. 2); around 100 cells were scored in four independent microscopy slide fields. Scale bar: 5 μm.

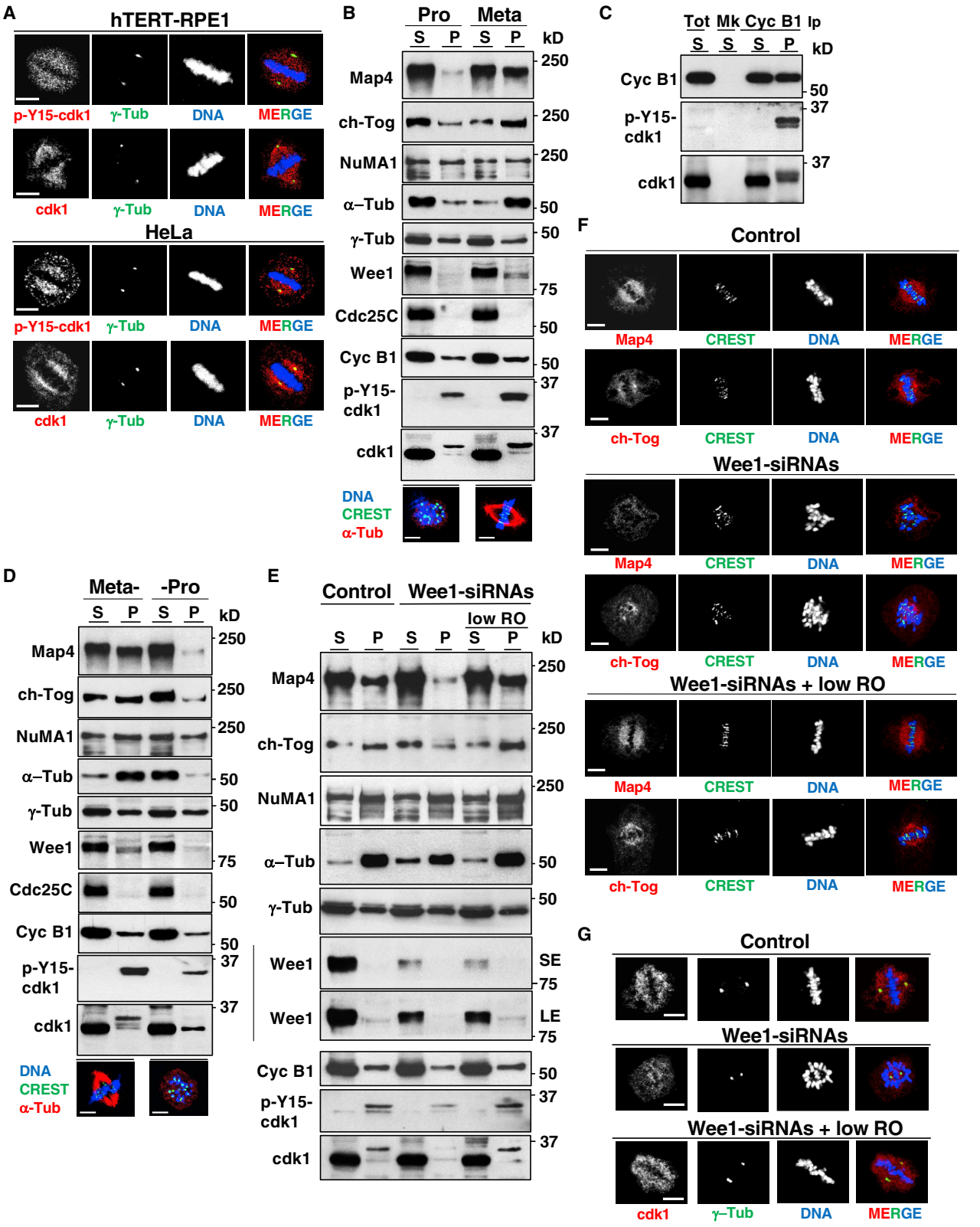

(legend on next page)

proteasome inhibitor MG-132 to block mitosis exit and the protein synthesis inhibitor cycloheximide (CHX) to prevent abnormal protein accumulation (M/C medium), the majority of control cells built normal bipolar spindles within 60-min incubation and remained stable for a further 20-min incubation (Figure 1A). Conversely, spindle assembly was markedly impaired in Wee1-downregulated cells, with defects that ranged from monopolarity to poorly structured bipolar spindles with gross chromosome alignment abnormalities (Figure 1A). To establish whether impaired spindle assembly was due to Wee1 loss per se or because it affected Cdk1 activity, we asked if mild Cdk1 inhibition could restore spindle assembly in Wee1-downregulated cells. Indeed, addition of RO-3306 at 0.5 μM (low-RO), from 60 to 80 min post G2 release, substantially restored spindle assembly (Figure 1A). Defects in spindle assembly were also induced by cdk1AF overexpression under similar conditions of G2-arrest and release, paralleling what was described by Krek and Nigg in 1991, as well as in Wee1-siRNA-treated HeLa cells or by chemical inhibition of Wee1, and in all cases, defects were substantially reversed by low-RO (Krek and Nigg, 1991; Serpico et al., 2019; Figures S2, S3 and S4A). In another set of experiments, non-targeting-siRNA-, as control, and Wee1-siRNA-treated hTERT-RPE1 cells were arrested at prometaphase by the reversible microtubule inhibitor nocodazole added shortly after siRNA treatments. Cells were, then, released in M/C medium for 80 min and a portion of Wee1-siRNA-treated cells also received low-RO at 60 min incubation. Within this period, the majority of control cells assembled spindles, while assembly was strongly impaired in Wee1-siRNA-treated cells but restored by low-RO (Figure 1B). When cells were released just into fresh medium, mitosis exit was delayed in Wee1-siRNA-treated cells, as shown by delayed cyclin B1 degradation, presumably by the action of the spindle assembly checkpoint (SAC; Serpico and Grieco, 2020; Figure S4C). Together, these data suggest that inhibitory phosphorylation-dependent control of Cdk1 activity is required for spindle assembly.

Localization of i-Cdk1

To directly test if a fraction of Cdk1 inhibited by phosphorylation, i-Cdk1, was present in mitotic cells and where it was localized, we probed metaphase cells with an antibody recognizing cdk1 phosphorylated at tyrosine 15 (p-Y15-cdk1; Figure 2A). The p-Y15-cdk1 signal appeared decorating the spindle area paralleling total cdk1 localization (Figure 2A). To biochemically dissect localization and function of mitotic i-Cdk1, we adapted a method described by Nigg and coworkers to isolate mitotic spindles and tightly associated proteins by separating the microtubular, insoluble, pellet fraction (P) from the soluble fraction (S) of mitotic cells (Silljé and Nigg, 2006). Nocodazole-treated, prometaphase-arrested hTERT-RPE1 cells were collected, released in M/C medium and taken at time 0 (prometaphase cells; Pro; Figure 2B) or after further 60-min incubation, to have metaphase cells (metaphase cells; Meta; Figure 2B). Cells were fractionated and proteins from soluble and pellet fractions analyzed (pellet fraction proteins were extracted in a buffer volume equivalent to one-fourth of the soluble fraction volume; then, equal volumes of soluble and pellet fractions were loaded on gels, so pellet proteins were enriched approximately 4-fold over soluble proteins relative to the distribution within a cell; see STAR Methods; Figure 2B). In the prometaphase cell pellet fraction, centrosomes were present as indicated by significant amounts of the central protein γ-tubulin and nuclear and mitotic apparatus protein 1 (NuMA1), a centrosome-associated protein (Mchedlishvili et al., 2018; Figure 2B). Conversely, α-tubulin was substantially present in the soluble fraction and much less in the pellet fraction, as expected because of the lack of spindle assembly, as well as the MAPs Map4 and ch-Tog (Figure 2B). In metaphase cells, instead, α-tubulin and significant amounts of Map4 and ch-Tog, the latter also involved in activating centrosome-independent, intra-spindle, microtubule nucleation, were present in the pellet fraction, reflecting spindle assembly (David et al., 2019; Thawani et al., 2020; Figure 2B). Distribution of NuMA1 and γ-tubulin in soluble and pellet fractions did not substantially change between prometaphase and metaphase cells (Figure 2B). The pellet fractions also contained small amounts of Wee1 that increased in metaphase cells, while minimal amounts of Cdc25C were equally present in pellet fractions from both prometaphase and metaphase cells (Figure 2B; similar protein distribution was found in HeLa cells under similar experimental conditions; see Figure S5). Small amounts of cyclin B1 and cdk1 were present in the pellet fraction of prometaphase cells and more of metaphase cells (Figure 2B). However, i-Cdk1 was found quite exclusively in pellet fractions, as shown by p-Y15-cdk1 signal and by retarded cdk1 mobility on SDS/PAGE, and more from metaphase than from prometaphase cells (Solomon et al., 1992; Figure 2B). Densitometric quantitation of the upshifted cdk1 forms on blots from metaphase cell pellet fraction indicated that i-Cdk1 represents less than 10% of total Cdk1. The selective presence of i-Cdk1 in the pellet fraction was confirmed also by probing immunoprecipitates of comparable amounts of cyclin B1 from soluble and pellet fractions of metaphase cells (Figure 2C).

In the metaphase cell pellet fraction, Map4 and ch-Tog appeared to have increased mobility on SDS/PAGE compared

Figure 2. i-Cdk1 localizes at spindle structures and is required for spindle assembly

(A) Growing hTERT-RPE1 and HeLa cells were treated for 20 min with MG-132, fixed, and stained for indicated antigens (γ-Tub; γ-tubulin).

(B) Prometaphase-arrested hTERT-RPE1 cells were released in M/C medium and taken at time 0 of incubation (prometaphase cells; Pro) or after further 60 min of incubation (metaphase cells; Meta). Soluble (S) and pellet (P) fractions were probed for indicated antigens. Bottom: immunofluorescence pictures of representative cells probed for indicated antigens.

(C) Cyclin B1 immunoprecipitates (Ips; Cyc B1 Ips) from Meta cell S and P fractions probed for indicated antigens (Mk: mock Ips).

(D) Meta cells obtained as described in (B) were further treated with vehicle (Meta-) or nocodazole (-Pro) from 60 min to 80 min of incubation. S and P fractions were probed for indicated antigens. Bottom: immunofluorescence pictures of representative cells stained for CREST (green), α-tubulin (red), and DNA (blue).

(E–G) hTERT-RPE1 cells were treated with non-targeting-siRNAs (Control) and Wee1-siRNAs, prometaphase-arrested and released in M/C medium for 80 min incubation, as described in Figures 1B and 1A, portion of Wee1-siRNA-treated cells received low-RO at 60 min post release. (E) S and P fractions probed for indicated antigens (for Wee1 short, SE, and long, LE, blot exposures are shown); (F, G) Cells were fixed and stained for indicated antigens. Scale bar: 5 μm.

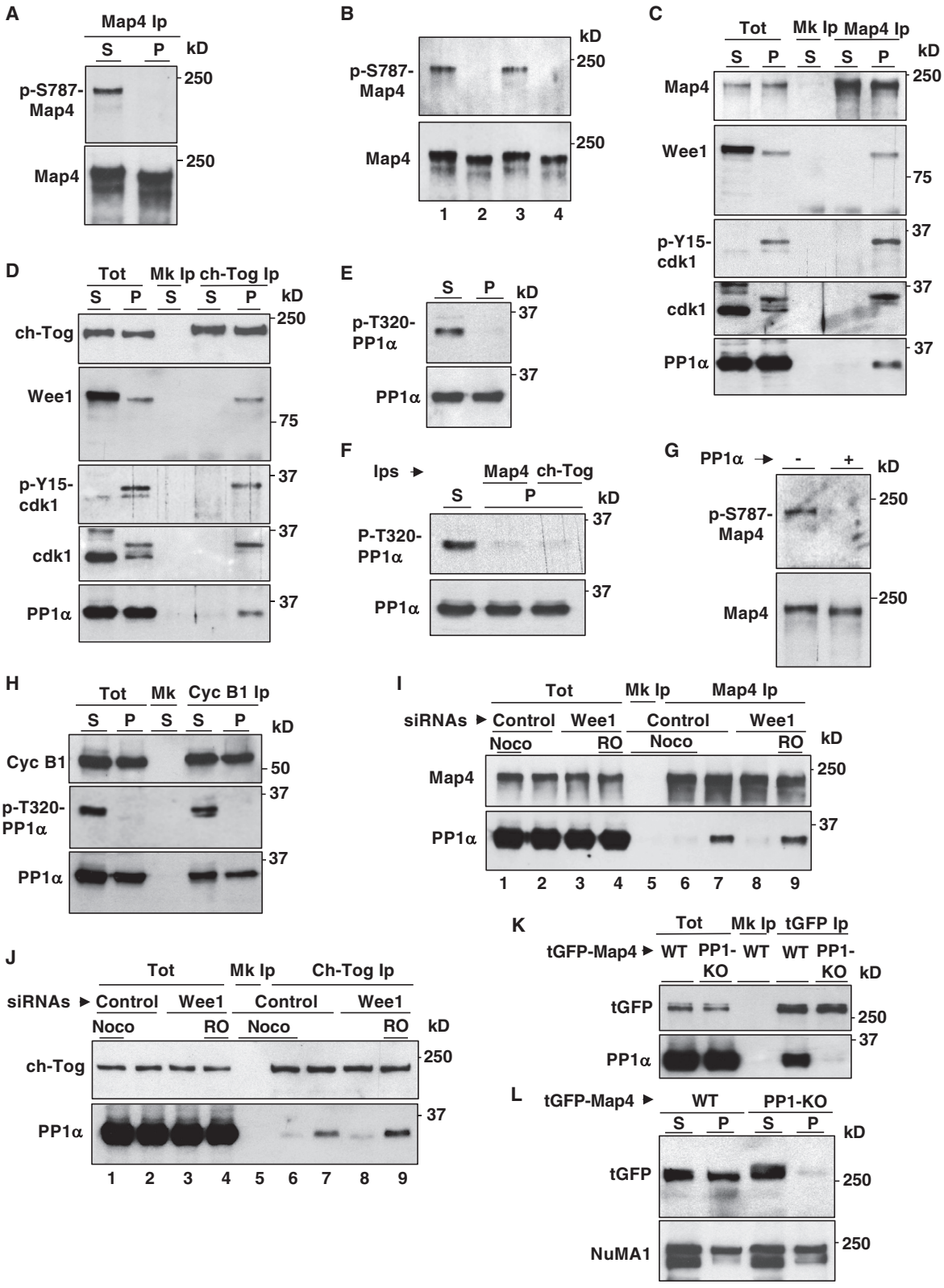

(legend on next page)

with soluble fraction, suggesting that these proteins were relatively dephosphorylated when microtubule bound. Indeed, when metaphase cells were further treated with nocodazole, from 60 to 80 min, to revert to a prometaphase condition, distribution of proteins between soluble and pellet fractions returned similar to prometaphase cells; Map4 and ch-Tog regained slower migration on SDS/PAGE, presumably reflecting their rephosphorylation when returning into the cytoplasm, while Wee1 and i-Cdk1 were reduced in the pellet fraction, indicating their dependence also on microtubule polymerization (Figure 2D). To ask whether a cause-effect relationship existed between i-Cdk1 and the control of Map4 and ch-Tog dephosphorylation and distribution, prometaphase-arrested control and Wee1-siRNA-treated cells were released into M/C medium as described in Figure 1B. Cells were further fractionated and the soluble and pellet fractions analyzed (Figure 2E). Control cells showed a similar distribution as in metaphase cells described in Figures 2B and 2D. In Wee1-siRNA-treated cells, the distribution of γ-tubulin and NuMA1 between the soluble and pellet fractions was similar to control cells; however, Map4, ch-Tog, and even part of α-tubulin were substantially less present in the pellet fraction relatively to control cells, a distribution pattern similar to that of prometaphase cells described in Figures 2B and 2D (Figure 2E). Addition of low-RO to Wee1-siRNA-treated cells reversed protein distribution relocating Map4, ch-Tog, and α-tubulin from the soluble to the pellet fraction like in control cells (Figure 2E). As expected, i-Cdk1 was reduced in Wee1-dowregulated cell pellet fraction compared with controls. However, addition of low-RO induced accumulation of part of residual Wee1, which escaped siRNA-mediated downregulation, in the pellet fraction and restored i-Cdk1 content (Figure 2E; note Wee1 in short, SE, and long exposures, LE). No increase of p-Y15-cdk1 signal was detected in the soluble fraction upon low-RO addition, indicating that small fluctuations of Cdk1 activity are indeed buffered in the cytosol by strong hysteresis and bistability of the Cdk1 autoactivatory loops, while nucleating spindle microtubules appeared insulated from them (Hunt, 2013; Novák and Tyson, 2021; Pomerening et al., 2003; Figure 2E). Localized inhibition of endogenous Cdk1 by low-RO treatment could possibly explain spindle assembly restoration in cdk1AF-expressing cells (Figure S2). Immunofluorescence analysis confirmed that Map4, ch-Tog, as well as cdk1 poorly localized to defectively structured spindles in Wee1-downregulated cells in a low-RO-reversible manner (Figures 2F and 2G). Poor localization of cdk1 at defective spindles was also evident in Wee1-downregulated HeLa cells and in hTERT-RPE1 cells expressing cdk1AF upon downregulation of endogenous cdk1 (Figures S6A and S6B). Similar mitotic defects and changes in protein distribution were induced by the chemical Wee1 inhibitor AZD1775 upon release from prometaphase-arrest, also in this case corrected by low-RO (Figure S4B). Together, these data indicate that i-Cdk1 is localized at spindle structures and required for proper mitotic spindle assembly and spindle microtubule association of Map4 and ch-Tog.

Spindle-localized MAP dephosphorylation and interaction with active PP1 depend on i-Cdk1

Microtubule growth- and stability-promoting properties of MAPs like ch-Tog and Map4 are antagonized by direct Cdk1 phosphorylation (Lieuvin et al., 1994; Mchedlishvili et al., 2018; Chang et al., 2001; Vasquez et al., 1999; Ookata et al., 1995). We were intrigued by the fact that changes in migration on SDS/PAGE suggested that these MAPs were hypophosphorylated when associated with spindle microtubules (see Figures 2B and 2D). We developed an anti-phosphospecific antibody recognizing phosphorylated Map4-serine 787 (p-S787-Map4), a target site for inhibition by Cdk1 *in vivo* (Ookata et al., 1997). Indeed, when the fusion proteins tGFP-Map4-wild type (WT) and tGFP-Map4-S787A (S787A), in which Map4 serine 787 was mutated into non-phosphorylatable alanine, were expressed and isolated from mitotic cells, the antibody recognized wild type but not the mutant version (Figure S7). Probing immunoprecipitates of comparable amounts of endogenous Map4 from soluble and pellet fractions of Meta cells for p-S787-Map4 showed that the signal was readily detected from the soluble fraction while hardly from the pellet fraction (Figure 3A). In addition, treating Map4 isolated from the pellet fraction with active Cdk1, *in vitro*, restored strong p-S787-Map4 signal and slower Map4 migration (Figure 3B). These data indicate that Map4 is dephosphorylated at Cdk1-dependent sites when bound to microtubules. Map4 and ch-Tog have been shown to physically interact with Cdk1, mediating association of the kinase with microtubules (Ookata et al., 1995; Charrasse et al., 2000). Our data from Wee1 downregulation experiments

Figure 3. i-Cdk1 assists spindle-localized MAP interaction with PP1 and dephosphorylation

From Meta hTERT-RPE1 cells:

(A) Map4 Ips from S and P fractions were probed for indicated antigens.

(B) Map4 Ips from S fraction (lane 1) and from P fraction (lanes 2–4) of Meta cells were incubated in kinase reaction buffer at 37°C for 15 min in the absence (lane 1 and 2) or in the presence of active Cdk1 without (lane 3) or with (lane 4) RO-3306. After incubation, Ips were probed for indicated antigens.

(C and D) (C) Map4 Ips and (D) ch-Tog Ips from S and P fractions were probed for indicated antigens (Tot: total samples; Mk Ips: mock Ips).

(E) Total S and P fractions were probed for indicated antigens.

(F) Total S fraction and Map4 and ch-Tog Ips from P fraction were probed for indicated antigens.

(G) Map4 Ips from S fraction were incubated in phosphatase reaction buffer at 37°C for 15 min in – or + active PP1α, then probed for indicated antigens.

(H) Cyclin B1 Ips from Meta cell S and P fractions probed for indicated antigens (Tot: total fractions; Mk: mock Ips).

(I and J) Non-targeting-siRNA- (Control) and Wee1-siRNA-treated (Wee1) hTERT-RPE1 cells released from prometaphase-arrest into M/C medium for 80 min incubation. A sample of control cells received nocodazole at time 0 (Noco), and a sample of Wee1-siRNAs cells received low-RO at 60 min of incubation (RO). Cells were lysed in high salt buffer and (I) Map4 or (J) ch-Tog Ips, lanes 6–9, were probed for indicated antigens (lanes 1–4: total lysate; lane 5: mock Ips from Noco cell lysates, Mk Ip).

(K and L) hTERT-RPE1 cells were transfected with tGFP-Map4-wild type (WT) and tGFP-Map4-PP1-KO expression vectors, arrested at metaphase and either (K) lysed in high salt buffer, then tGFP Ips performed and probed for indicated antigens, or (L) S and P fraction were isolated and probed for indicated antigens.

suggested that ch-Tog and Map4 distribution in the pellet fraction depended on i-Cdk1 (see Figure 2E). Indeed, immunoprecipitates of comparable amounts of Map4 or ch-Tog from the soluble and pellet fraction of metaphase cells showed that the MAPs selectively interacted with Wee1 and i-Cdk1 in the pellet fraction (Figures 3C and 3D). Together, these observations suggest that i-Cdk1 interacted with hypophosphorylated forms of these MAPs (Figures 3A, 3C, and 3D). In mitosis, major protein phosphatases like PP1 and PP2A are directly or indirectly inhibited by Cdk1 (Hunt, 2013). PP1 catalytic subunit is directly inhibited by Cdk1 phosphorylation, in particular the alpha isoform, PP1α, at threonine 320 (p-T320-PP1α), and phosphorylation at analogous sites inhibits other PP1 isoforms (Kwon et al., 1997). PP1 can, however, rapidly autoactivate by dephosphorylating itself, provided no Cdk1 activity in the proximity (Kwon et al., 1997). In addition to being catalytically active, PP1 often interacts with its substrates through specific domains to dephosphorylate them (Meadows et al., 2011; Häfner et al., 2014). Thus, first we asked whether PP1 interacted with Map4 and ch-Tog and found that the MAPs interacted with PP1α only in the pellet fraction (Figures 3C and 3D). Because of the presence of i-Cdk1, we hypothesized that PP1α in the pellet fraction was dephosphorylated at the Cdk1 inhibitory site. Indeed, when comparable amounts of PP1α were analyzed from soluble and pellet fractions of metaphase cells, the p-T320-PP1α signal was substantially detectable in the soluble fraction and barely in the pellet (Figure 3E). Probing comparable amounts of PP1α from total soluble fraction and from Map4 and ch-Tog immunoprecipitates showed that MAP-associated PP1α was dephosphorylated at the inhibitory Cdk1-dependent site (Figure 3F). Moreover, active PP1α was able to dephosphorylate Map4-S787 *in vitro* (Figure 3G).

Evidence of physical interaction between Cdk1 and PP1 has also been already reported, albeit in a rather different experimental context (Kim et al., 2018). By probing immunoprecipitates of comparable amounts of cyclin B1 from soluble and pellet fractions of metaphase cells, we found that PP1α substantially bound Cdk1 in both soluble and pellet fractions. However, cyclin B1-associated PP1α was phosphorylated at the inhibitory T320 in the soluble fraction but completely dephosphorylated at that site in the pellet fraction (Figure 3H). Thus, in the soluble fraction of mitotic cells, active Cdk1 is mostly bound to inactive PP1α; conversely, in the pellet fraction, i-Cdk1 binds the active form of PP1α. Moreover, when prometaphase-arrested control-siRNA- and Wee1-siRNA-treated cells were released into M/C medium for 80 min, PP1α was readily detectable in Map4 and ch-Tog immunoprecipitates from total extracts of control but not of Wee1-siRNA-treated cells that had reduced i-Cdk1 (Figures 3I and 3J, lanes 7 and 8; see Figure 2E). Addition of low-RO to Wee1-siRNA-treated cells, which restored i-Cdk1 and spindle assembly (see Figures 1B and 2E), also restored efficient PP1α binding to Map4 and ch-Tog (Figures 3I and 3J, lane 9). Thus, i-Cdk1 promotes localized PP1 activation and interaction with microtubule-stabilizing MAPs like Map4 and ch-Tog. The Map4 sequence KDVRW (from aa 318 to 322) matched a rather conserved PP1 binding motif (Meadows et al., 2011; R/KxVxF/W; where x is any aa). We mutated it into KDARA in tGFP-Map4-WT expression vector to produce tGFP-Map4-PP1-KO, a mutant impaired in PP1 binding. Indeed, when tGFP-Map4-WT and tGFP-Map4-PP1-KO were expressed at comparable levels and isolated from metaphase cells, PP1α substantially bound tGFP-Map4-WT but not tGFP-Map4-PP1-KO (Figure 3K). When the distribution in soluble and pellet fractions of tGFP-Map4-WT- and tGFP-Map4-PP1-KO-transfected metaphase cells was analyzed, tGFP-Map4-WT was readily detectable in the pellet fraction, while tGFP-Map4-PP1-KO remained substantially in the soluble fraction (Figure 3L). We concluded that i-Cdk1 allows localized activation of PP1 that can now interact with microtubule-stabilizing MAPs to dephosphorylate them and restore their microtubule growth-promoting properties.

Interdependence between i-Cdk1 and spindle formation

In complex with i-Cdk1, active PP1 appears to escape inhibitory phosphorylation by the largely active Cdk1 pool in mitotic cell cytoplasm. To gain further information on how i-Cdk1-associated PP1 resisted inhibitory phosphorylation by soluble active Cdk1, we challenged cyclin B1 immunoprecipitates from metaphase cell pellet fraction with soluble, recombinant, active Cdk1 *in vitro*. We found that the associated PP1α could not be phosphorylated at the inhibitory T-320 by soluble active Cdk1 (Figure 4A, compare lanes 5 and 6). Exogenous, recombinant, PP1α added to the same reaction was instead readily phosphorylated (Figure 4A, lane 7; recombinant PP1α was not phosphorylated at T320 unless treated *in vitro* with active Cdk1; Figure S8A). Similar results were obtained by immunoprecipitating i-Cdk1 with an anti-cdk1 antibody, thus making it unlikely that PP1 bound to i-Cdk1 was shielded from active Cdk1 by the precipitating antibody (Figure S8B). In addition, Map4 coimmunoprecipitating with cyclin B1 from metaphase cell pellet fraction, which represents a small fraction of total Map4 present in that fraction, resisted as well to phosphorylation by active Cdk1 *in vitro* (Figure 4B). Together, these data suggest that either other factors that shield the i-Cdk1 complexes from active Cdk1 were present in the immunoprecipitates and/or that interaction of i-Cdk1 with PP1 and MAPs is rather strong and perhaps these substrates cannot be phosphorylated by active Cdk1 unless they dissociated from i-Cdk1. Perhaps other factors, including the affinity of MAPs for microtubules, are necessary to release dephosphorylated MAPs from the complex with i-Cdk1-PP1 for their subsequent association with growing microtubules.

Probing cyclin B1 immunoprecipitates from soluble and pellet fractions of metaphase cells, shown in Figure 2C, for γ-tubulin revealed that it interacted with Cdk1 in pellet fraction (Figure 4C). Moreover, probing γ-tubulin immunoprecipitates from soluble and pellet fraction of prometaphase cells showed that it selectively interacted with i-Cdk1 and Wee1 in the pellet fraction (Figure 4D). Likely, centrosomes and γ-tubulin-dependent intraspindle microtubule nucleation contribute to the spindle-bound i-Cdk1 and Wee1 contents (David et al., 2019; Thawani et al., 2020; see Figures 4C and 4D). Nevertheless, i-Cdk1 and Wee1 appeared to increase in the pellet fraction of metaphase cells relative to that of prometaphase cells, suggesting a mutual relationship between microtubule polymerization and i-Cdk1 formation (see Figures 2B and 2D). Indeed, when the repartition of the Cdk1 inhibitory pathway players between soluble and pellet fractions of prometaphase and metaphase cells was probed on blots

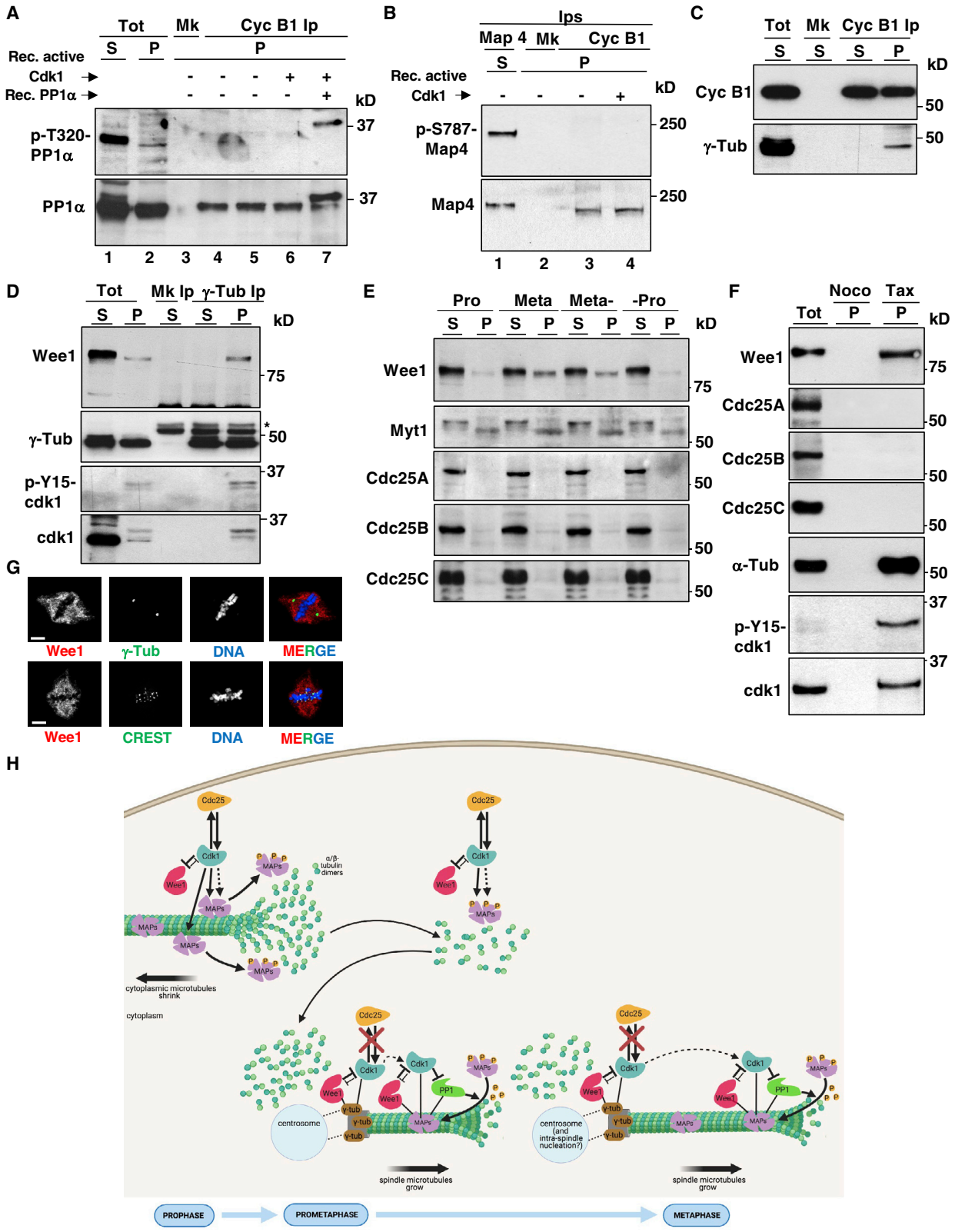

(legend on next page)

where higher amounts of pellet fraction proteins were loaded, it appeared more evident that the pellet fraction of metaphase cells had a higher Wee1 content than the pellet fraction of prometaphase cells. Myt1 also increased albeit to a lesser extent (Figure 4E). On parallel blots, no changes in distribution between metaphase and prometaphase cell fractions were, instead, detected for Cdc25 phosphatase family members (Figure 4E). Thus, polymerizing spindle microtubules appeared to bind Wee1 but not Cdc25, insulating Cdk1 from the cytoplasmic autoactivatory feedback loops and further promoting i-Cdk1 formation (Hunt, 2013; Novák and Tyson, 2021; Pomerening et al., 2003; Figure 4E). To corroborate the hypothesis that nucleating microtubules compartmentalized the Cdk1 control fostering i-Cdk1 formation, we used concentrated cytoplasmic extracts from prometaphase HeLa cells that were incubated with nocodazole or with the microtubule stabilizer taxol for 20 min at 23°C, the pellets were then eluted and analyzed (Meadows et al., 2011). The microtubular pellets, from taxol-treated extracts, aggregated with Wee1 and i-Cdk1 but not with Cdc25 family members (Figure 4F). The presence of Wee1 on spindles in cells was also confirmed by immunofluorescence analysis (Figure 4G).

DISCUSSION

Our data indicate that execution of mitosis relies on a compartmentalized control of Cdk1 activity. In mitosis, the large pool of Cdk1 is active and sustained by positive feedback loops (Hunt, 2013) to provide time and space for spindle assembly. Cdk1 activity provides time for spindle assembly by sustaining the SAC, which inhibits degradative Cdk1 inactivation until the metaphase-to-anaphase transition, and space by clearing the cytoplasm of microtubules for safe chromosome movements during spindle assembly, at least in part through inhibition of microtubule-stabilizing MAPs (Lieuvin et al., 1994; Ookata et al., 1995; Vasquez et al., 1999; Chang et al., 2001; D'Angiolella et al., 2003; Mchedlishvili et al., 2018; Alfonso-Pérez et al., 2019; Hayward et al., 2019; Allan et al., 2020; Serpico and Grieco, 2020). We show here that formation of the mitotic spindle, however, requires that a small fraction of Cdk1 remains inhibited by Wee1-dependent phosphorylation in mitosis, insulated from the positive feedback loops (Figure 4H). This fraction localizes at centrosomes and their nucleating microtubules and increases during spindle microtubule growth by further recruitment of Wee1 (David et al., 2019; Mchedlishvili et al., 2018; Thawani et al., 2020; Woodruff et al., 2017; see Figures 4E and 4H). Inhibited Cdk1 promotes PP1 activation and interaction with microtubule-stabilizing MAPs to locally reverse their inhibitory phosphorylation and promote spindle microtubule growth (Figure 4H). Until stable attachments with chromosomes are established, spindle microtubules can be rapidly destabilized perhaps also in virtue of the milieu of active Cdk1, making spindle assembly a highly dynamic process (Verde et al., 1990). How spindle microtubules are finally stabilized upon correct microtubule-kinetochore attachments is still unknown (Santaguida and Musacchio, 2009). Active Cdk1 localized at unattached kinetochores is also important to sustain the SAC, and whether stable microtubule-chromosome attachments and timely SAC silencing involve inhibitory phosphorylation of kinetochore-localized Cdk1 remain open questions (Alfonso-Pérez et al., 2019; Allan et al., 2020; Hayward et al., 2019; Serpico and Grieco, 2020). Previous evidence indicated that Cdk1-inhibitory proteins like Cdc6 and p21 could affect some mitotic events, so compartmentalized control of Cdk1 activity might also be contributed in part by these proteins in addition to inhibitory phosphorylation (Yim and Erikson, 2010; Schmidt et al., 2021). Together, our data show that execution of mitosis requires the concomitant and compartmentalized presence of active and inactive Cdk1 complexes to control the phosphorylation status and function of specific substrates in space and time.

Limitations of the study

The study is limited to two human cultured cells: hTERT-RPE1 (diploid; non-transformed retinal pigment epithelial) and HeLa (aneuploid; cervical cancer). Confirmation of these observations in other cell types or in *in vivo* models will be required to

Figure 4. Nucleating microtubules bind and foster i-Cdk1

(A) Lanes 1, 2: total S and P fractions of Meta hTERT-RPE1 cells; lane 3: mock Ips from P fraction; lanes 4–7: cyclin B1 Ips from P fractions; lane 4: Ips were immediately mixed with loading buffer; lanes 5–7: Ips were incubated in kinase reaction buffer at 37°C for 15 min in the absence (lane 5) or presence (lane 6) of recombinant, active, Cdk1 (+Rec. active Cdk1) and (lane 7) with recombinant, active, Cdk1 and recombinant PP1α (+Rec. active Cdk1 + Rec. PP1α). Samples were first probed for p-T320-PP1α, then for PP1α.

(B) Map 4 Ips from S fraction of Meta cells (lane1); mock Ips (lane 2; Mk) and cyclin B1 Ips from P fraction of Meta cells (lanes 3 and 4) were incubated in kinase reaction buffer at 37°C for 15 min in the absence (lane 1–3) or presence (lane 4) of recombinant, active, Cdk1 (+Rec. active Cdk1). Ips were then probed for indicated antigens.

(C) Cyclin B1 Ips described in Figure 2C were probed for γ-tubulin (Mk: mock Ips).

(D) Ips of comparable amounts of γ-tubulin from S and P fraction of Pro hTERT-RPE1 cells were probed for indicated antigens (the asterisk indicates signals generated by immunoglobulins in the Ips).

(E) S and P fraction from Pro, Meta, Meta-, and -Pro, as described in Figures 2B and 2D, were probed for indicated antigens on blots in which the P fraction was enriched 10-fold over S fraction (see STAR Methods).

(F) Eluates from pellets of mitotic HeLa cell extracts (P) incubated with nocodazole (Noco) or taxol (Tax) were probed for indicated antigens (Tot: 1/20 of total extract).

(G) Growing hTERT-RPE1 cells were treated for 20 min with MG-132, fixed, and stained for indicated antigens. Scale bar: 5 μm.

(H) A synoptic scheme depicting Cdk1 activity control in mitosis. At prophase, Cdk1 activity, sustained by positive feedback loops in the cytoplasm, destabilizes cytoplasmic microtubules by directly (continuous arrow) or indirectly (dashed arrow) phosphorylating MAPs. Centrosomes, however, maintain/promote inhibitory phosphorylation of a small Cdk1 fraction by selectively interacting with Wee1 and excluding Cdc25. From prometaphase to metaphase, further interaction of Wee1, inhibited Cdk1 and active PP1 with microtubule-stabilizing MAPs expands from centrosomes, and possibly from intra-spindle γ-tubulin-dependent nucleating centers, to promote reversal of inhibitory MAP phosphorylation and spindle microtubule growth.

generalize the study conclusions. Reconstitution of the i-Cdk1 complexes with PP1 and MAPs using recombinant proteins *in vitro*, although technically challenging because of the involvement of several players, will be required to better elucidate the molecular details of this basic spindle assembly control.

STAR★METHODS

Detailed methods are provided in the online version of this paper and include the following:

- KEY RESOURCES TABLE
- RESOURCE AVAILABILITY
  - Lead contact
  - Materials availability
  - Data and code availability
- EXPERIMENTAL MODEL AND SUBJECT DETAILS
  - Cell lines and cell culture
  - Transfection, RNA interference
  - Cell treatments
- METHOD DETAILS
  - DNA and siRNA constructs
  - Cell fractionation and extracts
  - Antibodies
  - Immunoprecipitation
  - Phosphorylation and dephosphorylation assays
  - Immunoblotting
  - Immunofluorescence fixation and staining
  - Microscopy
- QUANTIFICATION AND STATISTICAL ANALYSIS
  - Statistical analysis
  - Reproducibility
  - Image analysis and quantification

SUPPLEMENTAL INFORMATION

Supplemental information can be found online at https://doi.org/10.1016/j.celrep.2022.110305.

ACKNOWLEDGMENTS

The authors acknowledge V. E. Avvedimento for suggestions and R. Visconti and A. Romano for technical advice. D.G. acknowledges AIRC, Associazione Italiana per la Ricerca sul Cancro, for support (IG grant 2017; Id. 19851 to D.G.).

AUTHOR CONTRIBUTIONS

A.F.S. and D.G. designed and performed experiments and analyzed data. C.P. and F.F. performed immunoblot and immunofluorescence experiments and analyzed data. D. G. wrote the manuscript. A.F.S. revised the manuscript. All authors read and approved the final manuscript.

DECLARATION OF INTERESTS

The authors declare no competing interests.

Received: May 24, 2021
Revised: October 14, 2021
Accepted: January 6, 2022
Published: February 1, 2022

REFERENCES

Alfonso-Pérez, T., Hayward, D., Holder, J., Gruneberg, U., and Barr, F.A. (2019). MAD1-dependent recruitment of CDK1-CCNB1 to kinetochores promotes spindle checkpoint signaling. J. Cell Biol. *218*, 1108–1117.

Allan, L.A., Camacho Reis, M., Ciossani, G., Huis In 't Veld, P.J., Wohlgemuth, S., Kops, G.J., Musacchio, A., and Saurin, A.T. (2020). Cyclin B1 scaffolds MAD1 at the kinetochore corona to activate the mitotic checkpoint. EMBO J. *39*, e103180.

Chang, W., Gruber, D.S., Kitazawa, H., Hamazumi, Y., Hisanaga, S., and Bulinski, J.C. (2001). Phosphorylation of MAP4 affects microtubule properties and cell cycle progression. J. Cell Sci. *114*, 2879–2887.

Charrasse, S., Lorca, T., Dorée, M., and Larroque, C. (2000). The Xenopus XMAP215 and its human homologue TOG proteins interact with cyclin B1 to target p34cdc2 to microtubules during mitosis. Exp. Cell Res. *254*, 249–256.

D'Angiolella, V., Mari, C., Nocera, D., Rametti, L., and Grieco, D. (2003). The spindle checkpoint requires cyclin-dependent kinase activity. Genes Dev. *17*, 2520–2525.

D'Angiolella, V., Palazzo, L., Santarpia, C., Costanzo, V., and Grieco, D. (2007). Role for non-proteolytic control of M-phase-promoting factor activity at M-phase exit. PLoS One *2*, e247.

David, A.F., Roudot, P., Legant, W.R., Betzig, E., Danuser, G., and Gerlich, D.W. (2019). Augmin accumulation on long-lived microtubules drives amplification and kinetochore-directed growth. J. Cell Biol. *218*, 2150–2168.

Gergely, F., Draviam, V.M., and Raff, J.W. (2003). The ch-TOG/XMAP215 protein is essential for spindle pole organization in human somatic cells. Genes Dev. *17*, 336–341.

Häfner, J., Mayr, M.I., Möckel, M.M., and Mayer, T.U. (2014). Pre-anaphase chromosome oscillations are regulated by the antagonistic activities of Cdk1 and PP1 on Kif18A. Nat. Commun. *5*, 4397.

Hagting, A., Karlsson, C., Clute, P., Jackman, M., and Pines, J. (1988). MPF localization is controlled by nuclear export. EMBO J. *17*, 4127–4138.

Hayward, D., Alfonso-Pérez, T., Cundell, M.J., Hopkins, M., Holder, J., Bancroft, J., Hutter, L.H., Novak, B., Barr, F.A., and Gruneberg, U. (2019). CDK1-CCNB1 creates a spindle checkpoint-permissive state by enabling MPS1 kinetochore localization. J. Cell Biol. *218*, 1182–1199.

Hunt, T. (2013). On the regulation of protein phosphatase 2A and its role in controlling entry into and exit from mitosis. Adv. Biol. Regul. *53*, 173–178.

Kim, H.J., Shin, J., Lee, S., Kim, T.W., Jang, H., Suh, M.Y., Kim, J.H., Hwang, I.Y., Hwang, D.S., Cho, E.J., and Youn, H.D. (2018). Cyclin-dependent kinase 1 activity coordinates the chromatin associated state of Oct4 during cell cycle in embryonic stem cells. Nucleic Acids Res. *46*, 6544–6560.

Krek, W., and Nigg, E.A. (1991). Mutations of p34cdc2 phosphorylation sites induce premature mitotic events in HeLa cells: evidence for a double block to p34cdc2 kinase activation in vertebrates. EMBO J. *10*, 3331–3341.

Kwon, Y.G., Lee, S.Y., Choi, Y., Greengard, P., and Nairn, A.C. (1997). Cell cycle-dependent phosphorylation of mammalian protein phosphatase 1 by cdc2 kinase. Proc. Natl. Acad. Sci. U S A *94*, 2168–2173.

Lieuvin, A., Labbé, J.C., Dorée, M., and Job, D. (1994). Intrinsic microtubule stability in interphase cells. J. Cell Biol. *124*, 985–996.

Mchedlishvili, N., Matthews, H.K., Corrigan, A., and Baum, B. (2018). Two-step interphase microtubule disassembly aids spindle morphogenesis. BMC Biol. *16*, 14.

Meadows, J.C., Shepperd, L.A., Vanoosthuyse, V., Lancaster, T.C., Sochaj, A.M., Buttrick, G.J., Hardwick, K.G., and Millar, J.B.A. (2011). Spindle checkpoint silencing requires association of PP1 to both Spc7 and kinesin-8 motors. Dev. Cell. *20*, 739–750.

Novák, B., and Tyson, J.J. (2021). Mechanisms of signalling-memory governing progression through the eukaryotic cell cycle. Curr. Opin. Cell Biol. *69*, 7–16.

Oh, J.S., Susor, A., and Conti, M. (2011). Protein tyrosine kinase Wee1B is essential for metaphase II exit in mouse oocytes. Science *332*, 462–465.

Ookata, K., Hisanaga, S., Bulinski, J.C., Murofushi, H., Aizawa, H., Itoh, T.J., Hotani, H., Okumura, E., Tachibana, K., and Kishimoto, T. (1995). Cyclin B interaction with microtubule-associated protein 4 (MAP4) targets p34cdc2 kinase to microtubules and is a potential regulator of M-phase microtubule dynamics. J. Cell Biol. *128*, 849–862.

Ookata, K., Hisanaga, S., Sugita, M., Okuyama, A., Murofushi, H., Kitazawa, H., Chari, S., Bulinski, J.C., and Kishimoto, T. (1997). MAP4 is the in vivo substrate for CDC2 kinase in HeLa cells: identification of an M-phase specific and a cell cycle-independent phosphorylation site in MAP4. Biochemistry *36*, 15873–15883.

Pomerening, J.R., Sontag, E.D., and Ferrell, J.E., Jr. (2003). Building a cell cycle oscillator: hysteresis and bistability in the activation of Cdc2. Nat. Cell Biol. *5*, 346–351.

Santaguida, S., and Musacchio, A. (2009). The life and miracles of kinetochores. EMBO J. *28*, 2511–2531.

Schmidt, A.K., Pudelko, K., Boekenkamp, J.E., Berger, K., Kschischo, M., and Bastians, H. (2021). The p53/p73 - $p21^{CIP1}$ tumor suppressor axis guards against chromosomal instability by restraining CDK1 in human cancer cells. Oncogene *40*, 436–451.

Serpico, A.F., D'Alterio, G., Vetrei, C., Della Monica, R., Nardella, L., Visconti, R., and Grieco, D. (2019). Wee1 rather than Plk1 is inhibited by AZD1775 at therapeutically relevant concentrations. Cancers *11*, 819.

Serpico, A.F., and Grieco, D. (2020). Recent advances in understanding the role of Cdk1 in the spindle assembly checkpoint. F1000Res. *9*, 50–57, F1000 Faculty Rev-57.

Silljé, H.H.W., and Nigg, E.A. (2006). Purification of mitotic spindles from cultured human cells. Methods *38*, 25–28.

Solomon, M.J., Lee, T., and Kirschner, M.W. (1992). Role of phosphorylation in p34cdc2 activation: identification of an activating kinase. Mol. Biol. Cell. *3*, 13–27.

Thawani, A., Rale, M.J., Coudray, N., Bhabha, G., Stone, H.A., Shaevitz, J.W., and Petry, S. (2020). The transition state and regulation of γ-TuRC-mediated microtubule nucleation revealed by single molecule microscopy. Elife *9*, e54253.

Vasquez, R.J., Gard, D.L., and Cassimeris, L. (1999). Phosphorylation by CDK1 regulates XMAP215 function in vitro. Cell Motil. Cytoskeleton *43*, 310–321.

Vassilev, L.T., Tovar, C., Chen, S., Knezevic, D., Zhao, X., Sun, H., Heimbrook, D.C., and Chen, L. (2006). Selective small-molecule inhibitor reveals critical mitotic functions of human CDK1. Proc. Natl. Acad. Sci. U S A *103*, 10660–10665.

Verde, F., Labbé, J.C., Dorée, M., and Karsenti, E. (1990). Regulation of microtubule dynamics by cdc2 protein kinase in cell-free extracts of Xenopus eggs. Nature *343*, 233–238.

Visconti, R., Della Monica, R., Palazzo, L., D'Alessio, F., Raia, M., Improta, S., Villa, M.R., Del Vecchio, L., and Grieco, D. (2015). The Fcp1-Wee1-Cdk1 axis affects spindle assembly checkpoint robustness and sensitivity to antimicrotubule cancer drugs. Cell Death Differ. *22*, 1551–1560.

Visconti, R., Palazzo, L., Della Monica, R., and Grieco, D. (2012). Fcp1-dependent dephosphorylation is required for M-phase-promoting factor inactivation at mitosis exit. Nat. Commun. *3*, 894.

Woodruff, J.B., Ferreira Gomes, B., Widlund, P.O., Mahamid, J., Honigmann, A., and Hyman, A.A. (2017). The centrosome is a selective condensate that nucleates microtubules by concentrating tubulin. Cell *169*, 1066–1077.

Yim, H., and Erikson, R.L. (2010). Cell division cycle 6, a mitotic substrate of polo-like kinase 1, regulates chromosomal segregation mediated by cyclin-dependent kinase 1 and separase. Proc. Natl. Acad. Sci. U S A. *107*, 19742–19747.

STAR★METHODS

KEY RESOURCES TABLE

REAGENT or RESOURCE	SOURCE	IDENTIFIER
Antibodies		
mouse anti-α-tubulin	Sigma-Aldrich	Clone DM1A; Cat# T9026; RRID: AB_477593
mouse anti-cdc2	BD Biosciences	Cat# 610038; RRID: AB_397454
rabbit anti-Cdc25C	Cell Signaling Technology	Cat# 4688; RRID: AB_560956
human anti-centromere (CREST)	Antibodies Incorporated	Cat# 15-234; RRID: AB_2687472
rabbit anti-ch-Tog	Abcam	Cat# ab86073; RRID: AB_1924889
rabbit anti-ch-Tog	Proteintech	Cat# 26457-1-AP; RRID: AB_2880520
rabbit anti-cyclin B1	Bethyl	Cat# A305-000A; RRID: AB_2621194
mouse anti-γ-tubulin	Sigma-Aldrich	Clone GTU-88; Cat# T5326; RRID: AB_532292
rabbit anti-γ-tubulin	Sigma-Aldrich	Cat# SAB4503045; RRID: AB_10747615
mouse IgG2b, Isotype Control	Abcam	Cat# abaf18469
rabbit IgG, Isotype Control	Abcam	Cat# ab172730; RRID: AB_2687931
rabbit anti-human IgG FITC conjugated	Dako Agilent	Cat# F005601; RRID: AB_578626
goat anti-human IgG rhodamine conjugated	Santa Cruz Biotechnology	Cat# sc2457; RRID: AB_648979
sheep anti-mouse IgG HRP linked	GE Healthcare	Cat# NA931; RRID: AB_772210
donkey anti-rabbit IgG HRP linked	GE Healthcare	Cat# NA934; RRID: AB_772206
goat anti-mouse IgG Alexa Fluor 488	Invitrogen	Cat# A11029; RRID: AB_2534088
donkey anti-mouse IgG Alexa Fluor 594	Invitrogen	Cat# A21203; RRID: AB_141633
donkey anti-rabbit IgG Alexa Fluor 488	Invitrogen	Cat# A21206; RRID: AB_2535792
donkey anti-rabbit IgG Alexa Fluor 594	Invitrogen	Cat# A21207; RRID: AB_141637
rabbit anti-Map4	Abcam	Cat# ab224543
rabbit anti-Map4	Bethyl	Cat# A301-488A; RRID: AB_999613
rabbit anti-Myt1	Cell Signaling Technology	Cat# 4282; RRID: AB_2163831
rabbit anti-NuMA	Novus Biologicals	Cat# NB100-74636; RRID: AB_1049265
rabbit anti-phospho-serine-787-Map4	CovalAb	N/A
rabbit anti-phospho-threonine-14-cdc2	Cell Signaling Technology	Cat# 2543; RRID: AB_823465
rabbit anti-phospho-threonine-320-PP1α	Cell Signaling Technology	Cat# 2581; RRID: AB_330823
rabbit anti-phospho-tyrosine-15-cdc2	Boster Bio	Cat# P00209
rabbit anti-phospho-tyrosine-15-cdc2	Cell Signaling Technology	Cat# 4539; RRID: AB_560953
mouse anti-PP1γ	Santa Cruz Biotechnology	Cat# sc-515943
mouse anti-turboGFP	OriGene	Clone 2H8; Cat# TA150041; RRID: AB_2622256
rabbit anti-Wee1	Cell Signaling Technology	Cat# 13084; RRID: AB_2713924
Bacterial and virus strains		
E. coli: MAX efficiency DH5α competent cells	Invitrogen	Cat# 18258012
Chemicals, peptides, and recombinant proteins		
Adavosertib (MK-1775, AZD1775)	Selleckchem	Cat# S1525
Cycloheximide (CHX)	Santa Cruz Biotechnology	Cat# sc-3508
MG-132	Calbiochem	Cat# 474790
Nocodazole, microtubule inhibitor	Abcam	Cat# ab120630
RO-3306, Cdk1 inhibitor IV	Calbiochem	Cat# 217699

(*Continued on next page*)

Continued

REAGENT or RESOURCE	SOURCE	IDENTIFIER
Taxol (paclitaxel)	Sigma-Aldrich	Cat# T1912
DharmaFECT 1 siRNA Transfection Reagent	Dharmacon	Cat# T-2001-03
MegaTran 2.0 Transfection Reagent	OriGene	Cat# TT210003
Polyethylenimine (PEI)	Polysciences	Cat# 23966
recombinant active Cdk1	Sigma-Aldrich	Cat# 14-450
recombinant human PP1α	Novus Biologicals	Cat# NBP1-72418
Critical commercial assays		
mouse anti-cyclin B1 agarose	Santa Cruz Biotechnology	Cat# sc245AC; RRID: AB_627338
mouse anti-turboGFP agarose	OriGene	Clone 2H8 Cat# TA183081; RRID: AB_2622344
protein A/G PLUS-agarose	Santa Cruz Biotechnology	Cat# sc-2003; RRID: AB_10201400
mouse anti-γ-tubulin agarose	Santa Cruz Biotechnology	Cat# sc-17788AC; RRID: AB_628418
normal mouse IgG-AC	Santa Cruz Biotechnology	Cat# sc-2343; RRID: AB_737178
Experimental models: Cell lines		
Human: HeLa cells	CEINGE Cell Culture Facility	N/A
Human: hTERT-RPE1 cells	Kind gift from Dr. A. Musacchio, Max Planck Institute of Molecular Physiology, Dortmund	N/A
Oligonucleotides		
siRNA targeting sequence: human Cdk1 #1: GAAAUUGAGCGGAGAGCGAUU	Dharmacon	N/A
siRNA targeting sequence: human Cdk1 #2: CGUAAUGCUUUGAAGUAUUUU	Dharmacon	N/A
siRNA targeting sequence: human Cdk1 #3: CAACCUGGCUAAAGAUGAAUU	Dharmacon	N/A
siRNA targeting sequence: human Cdk1 #4: GAUCAAGGGCUGUCCGCAAUU	Dharmacon	N/A
siRNA targeting sequence: human WEE1 #1: CUGUAAACUUGUAGCAUUAUU	Dharmacon	N/A
siRNA targeting sequence: human WEE1 #2: GUACAUAGCUGUUUGAAAUUU	Dharmacon	N/A
siRNA targeting sequence: human WEE1 #3: GGGCUUU AUUACAGACAUAUU	Dharmacon	N/A
Recombinant DNA		
tGFP-Map4-WT, vector: pCMV6-AC-GFP	OriGene	Cat# RG216364
tGFP-Map4-S787A, vector: pCMV6-AC-GFP	OriGene	N/A
tGFP-Map4-PP1-KO, vector: pCMV6-AC-GFP	OriGene	N/A
pcDNA3-cdc2WT, vector: pcDNA3.1	Hagting et al. (1998)	Addgene Cat# 61840; RRID: Addgene_61840
pcDNA3-cdc2AF, vector: pcDNA3.1	Hagting et al. (1998)	Addgene Cat# 39872; RRID: Addgene_39872
3XFlag-Wee1, vector: p3xFLAG-CMV-7.1	Visconti et al. (2012)	N/A
pCMV6-AC-GFP	OriGene	Cat# PS100010
pcDNA3.1	Invitrogen	Cat# V79020
p3xFLAG-CMV-7.1	Sigma-Aldrich	Cat# E7533

(*Continued on next page*)

Continued

REAGENT or RESOURCE	SOURCE	IDENTIFIER
Software and algorithms		
ImageJ	ImageJ;	https://imagej.nih.gov
ZEN 3.1	Zeiss	https://www.zeiss.com
BioRender	BioRender	https://biorender.com
Excel	Microsoft	https://microsoft.com

RESOURCE AVAILABILITY

Lead contact

Further information and requests for resources and reagents should be directed to and will be fulfilled by the lead contact, Domenico Grieco (domenico.grieco@unina.it).

Materials availability

Custom reagents generated in this study from CovaLab, Dharmacon, OriGene are available on request.

Data and code availability

All data reported in this paper will be shared by the lead contact upon request.

This paper does not report original code.

Any additional information required to reanalyze the data reported in this paper is available from the lead contact upon request.

EXPERIMENTAL MODEL AND SUBJECT DETAILS

Cell lines and cell culture

Human Henrietta Lacks (HeLa) cells were form CEINGE Cell Culture Facility. Human Telomerase Reverse Transcriptase- immortalized Retinal Pigment Epithelial (hTERT-RPE1) cells were a kind gift from Dr. A. Musacchio, Max Planck Institute of Molecular Physiology, Dortmund. Cells were not authenticated by authors and regularly checked for mycoplasma contamination using the CEINGE Cell Culture Facility services. HeLa cells were grown in Roswell Park Memorial Institute Medium (RPMI-1640; Sigma-Aldrich), hTERT-RPE1 cells were grown in Dulbecco's Modified Eagle Medium: Nutrient Mixture F-12 (DMEM/F12; Gibco, Thermo Fisher Scientific), both supplemented with 10% fetal bovine serum (FBS; Gibco), 1% GlutaMAX-supplement (Gibco), 1% penicillin/streptomycin (Euroclone), at 37°C with 5% CO_2.

Transfection, RNA interference

Transfections were performed using Polyethylenimine (PEI) (Polysciences) or MegaTran 2.0 Transfection Reagent (OriGene), for plasmids up to 8 kb in size or greater than 10 kb, respectively. Cells were seeded into 10 cm dishes and transfected after 24 hours, according to the manufacturer's protocol. Briefly, MegaTran (1 μg/μL) or PEI (1 μg/μL): DNA (1 μg/μL) (3:1) were mixed in RPMI-1640 or DMEM/F12 media and incubated at room temperature (rt) for 20 min, then, the mixture was added to the cells and incubated for 24 hours.

RNA interference via siRNAs was performed using DharmaFECT 1 siRNA Transfection Reagent (Dharmacon). For efficient knockdown cells were plated 24 hours prior to treatment and transfected with 25 nM of siRNAs duplex using DharmaFECT 1, according to the manufacturer's protocol. DharmaFECT 1 and siRNAs were mixed in RPMI-1640 or DMEM/F12 media and incubated at rt for 20 min, then, the mixture was added to the cells and incubated for 24 hours (see also cell treatments section).

Cell treatments

For cdk1-siRNA treatment and complementation experiments, cells were treated with non-targeting or specific siRNAs 12 hours before empty vector, cdk1 WT or cdk1 AF expression plasmid transfection. 8 hours post transfection, cells were incubated with nocodazole (Abcam) at 1 μg/mL and 100 ng/mL for further 16 or 14 hours of incubation for hTERT-RPE1 and HeLa cells, respectively, to have prometaphase-arrested cells. For Wee1-siRNA treatment and complementation experiments cells were transfected with mock- or 3XFlag-Wee1 expression construct-transfected 24 hours prior to treatment with non-targeting or specific siRNAs. For synchronization of siRNA-treated cells, 6 hours after siRNA-treatment, cells were incubated with RO-3306 at 9 μM (high-RO; Calbiochem) for further 16 hours of incubation, to have G2-arrested cells, or with nocodazole (Abcam) at 1 μg/mL and 100 ng/mL for further 16 or 14 hours of incubation for hTERT-RPE1 and HeLa cells, respectively, to have prometaphase-arrested cells. To obtain metaphase-arrested cells, prometaphase-arrested cells were collected and washed twice with fresh medium and twice with phosphate buffer saline (PBS; Euroclone) solution before plating into fresh medium containing MG-132 (20 μM; Calbiochem) and cycloheximide (CHX; 60 μg/mL; Santa Cruz Biotechnology) for further 60 min incubation. Reversal from metaphase to prometaphase condition

was obtained by adding nocodazole (-Pro; 1 μg/mL; Abcam) to metaphase cells by 60 min of incubation in MG-132 for further 20 min of incubation; control metaphase cells received dimethyl sulfoxide (DMSO; Sigma-Aldrich; Meta-). Where indicated AZD1775 (Selleckchem) was added at 1 μM. Mild inhibition of Cdk1 activity was obtained by adding RO-3306 at 0.5 μM (low-RO; Calbiochem).

METHOD DETAILS

DNA and siRNA constructs

Mammalian expression plasmids for turbo-GFP-Map4-wild type (tGFP-Map4-WT), turbo-GFP-Map4 rendered non-phosphorylatable at serine 787 (tGFP-Map4-S787A) and turbo-GFP-Map4 defective in PP1 binding Map4 (tGFP-Map4-PP1-KO), in which the Map4 peptide KDVRW (from aa 318 to 322; human Map4 isoform 1) was mutated into KDARA, were generated and purchased from OriGene. Cdk1WT and cdk1AF mammalian expression plasmids have been described before (Hagting et al., 1998) and were purchased from Addgene. 3XFlag-Wee1 expression construct was obtained as previously described (Visconti et al., 2012).

Custom siRNAs targeting the 5'-UTR of human Cdk1 (#1: 5'-GAAAUUGAGCGGAGAGCGAUU-3'), 3'-UTR of human Cdk1 (#2: 5'-CGUAAUGCUUUGAAGUAUUUU-3'; #3: 5'-CAACCUGGCUAAAGAUGAAUU-3'; #4: 5'-GAUCAAGGGCUGUCCGCAAUU-3'), the 3′-UTR of human WEE1 (#1: 5'-CUGUAAACUUGUAGCAUUAUU-3'; #2: 5'-GUACAUAGCUGUUUGAAAUUU-3'; #3: 5'-GGGCUUUAUUACAGACAUAUU-3') were designed using siDESIGN Center tool by Horizon and purchased from Dharmacon.

Cell fractionation and extracts

To isolate spindle-bound protein we adapted a previously described method (Silljé and Nigg, 2006). All the steps, except the final elution, were performed at rt to preserve microtubules. Cells were harvested by centrifugation and washed once with PBS containing taxol (1 μM; Sigma-Aldrich). 5 x 10^6 cells were resuspended in 800 μL of fractionation lysis buffer (FLB; 40 mM β-glycerophosphate, 15 mM $MgCl_2$, 20 mM EGTA, 0.25% Igepal, 20 mM Hepes, 5 μM taxol, 6 μg/mL latrunculin B; Sigma-Aldrich) supplemented with 300 μg/mL RNase A and 120 U/mL DNase I (Roche). After careful resuspension, samples were incubated in thermomixer (Eppendorf thermomixer comfort) at 34°C for 20 min with constant shaking at 1.200 rpm. Lysates were spun at 6.800 rpm (Eppendorf centrifuge 5425) for 2 min: the soluble fractions were collected and transferred into new tubes and supplemented with 250 mM NaCl and saved (soluble fraction). The pellet fractions were resuspended in FLB + 300 μg/mL RNase A and 120 U/mL DNase I and again incubated in thermomixer at 34°C for 20 min with constant shaking at 1.200 rpm. The pellets were collected again by centrifugation and were washed twice with washing buffer (WB; 5 mM Hepes, 5 μM taxol; Sigma-Aldrich). Finally, the pellet fraction proteins were extracted by resuspending pellets in 200 μL of FLB minus taxol and supplemented with 250 mM NaCl. Resuspended pellets were incubated on ice for 30 min and then spun at 4°C at 3.200 rpm for 10 min (Eppendorf centrifuge 5424 R), the supernatants spun again under identical condition and the final supernatants were collected (pellet fraction). Soluble and pellet fractions were further analyzed by immunoblottings (Ibs) or immunoprecipitations (Ips). Being the pellet fraction proteins extracted in a 200 μL buffer volume from a total cell lysate of 800 μL volume (mostly representing the soluble fraction volume), at equal fraction volumes, proteins from the pellet fraction were enriched 4 folds over the soluble fraction proteins, relatively to the distribution within cells. To induce microtubule polymerization and analyze microtubule-bound proteins in mitotic cell extracts, HeLa cell extracts were obtained as previously described (Visconti et al., 2012). Briefly, cells were synchronized at prometaphase by 14 hour nocodazole (Abcam) treatment. Detached cells were collected and washed once with ice-cold PBS and lysed in 75% pellet volume extraction buffer (20 mM HEPES, pH 7.6, 5 mM KCl, 1 mM dithiothreitol; Sigma-Aldrich) by three freeze–thaw cycles. Lysate was centrifuged at 13.200 rpm for 1 hour at 4°C and supernatant were supplemented with a 20X energy regeneration mix (1 mM ATP, 10 mM phosphocreatine and 0.1 mg/mL creatine phosphokinase; Sigma-Aldrich) and 1 mM GTP (Sigma-Aldrich). 50 μl aliquots were treated with nocodazole (1μg/mL; Abcam), as control, or taxol (5 μM; Sigma-Aldrich) for 20 min at rt, diluted 10 times with FLB and spun at 6.800 rpm (Eppendorf centrifuge 5425) for 2 min. The pellets were washed once more in FLB and finally resuspended in 30 μL FLB supplemented with 250 mM NaCl, incubated on ice for 30 min and then spun 13.200 rpm at 4 °C for 10 min (Eppendorf centrifuge 5424 R). Samples were then analyzed by Ibs; total samples = 5 μL of total mitotic extract.

Antibodies

Primary antibodies used in this study: mouse anti-α-tubulin, clone DM1A (Sigma-Aldrich, Cat# T9026; RRID: AB_477593), mouse anti-cdc2 (BD Biosciences, Cat# 610038, RRID: AB_397454), rabbit anti-Cdc25C (Cell Signaling Technology, Cat# 4688, RRID: AB_560956), human anti-centromere (CREST; Antibodies Incorporated, Cat# 15-234, RRID: AB_2687472), rabbit anti-ch-Tog (Abcam, Cat# ab86073, RRID: AB_1924889), rabbit anti-ch-Tog (Proteintech, Cat# 26457-1-AP, RRID: AB_2880520), rabbit anti-cyclin B1 (Bethyl, Cat# A305-000A, RRID: AB_2621194), mouse anti-γ-tubulin, clone GTU-88 (Sigma-Aldrich, Cat# T5326, RRID: AB_532292), rabbit anti-γ-tubulin (Sigma-Aldrich, Cat# SAB4503045, RRID: AB_10747615), mouse IgG2b, Isotype Control (Abcam, Cat# abaf18469), rabbit IgG, Isotype Control (Abcam, Cat# ab172730, RRID: AB_2687931), rabbit anti-human IgG FITC conjugated (Dako Agilent, Cat# F005601, RRID: AB_578626), goat anti-human IgG rhodamine conjugated (Santa Cruz Biotechnology, Cat# sc2457, RRID: AB_648979), sheep anti-mouse IgG peroxidase-(HRP) linked (GE Healthcare, Cat# NA931, RRID: AB_772210), donkey anti-rabbit IgG HRP-linked (GE Healthcare, Cat# NA934, RRID: AB_772206), goat anti-mouse IgG Alexa Fluor 488 (Invitrogen, Cat# A11029, RRID: AB_2534088), donkey anti-mouse IgG Alexa Fluor 594 (Invitrogen, Cat# A21203, RRID: AB_141633), donkey anti-rabbit IgG Alexa Fluor 488 (Invitrogen, Cat# A21206, RRID: AB_2535792), donkey anti-rabbit IgG Alexa Fluor 594

(Invitrogen, Cat# A21207, RRID: AB_141637), rabbit anti-Map4 (Abcam, Cat# ab224543), rabbit anti-Map4 (Bethyl, Cat# A301-488A, RRID: AB_999613), rabbit anti-Myt1 (Cell Signaling Technology, Cat# 4282, RRID: AB_2163831), rabbit anti-NuMA (Novus Biologicals, Cat# NB100-74636, RRID: AB_1049265). Rabbit polyclonal antibody against phosphorylate serine 787 of human Map4 (rabbit anti-phospho-serine-787-Map4; P-S787-Map4) was raised using C-DAKAPEKRA[Sp]PSKPA-coNH2 peptide as immunogen; peptide synthesis, rabbit inoculation, serum production and cross-affinity antibody purification were carried out by CovalAb. Rabbit anti-phospho-threonine-14-cdc2 (P-T14-cdc2; Cell Signaling Technology, Cat# 2543, RRID: AB_823465), rabbit anti-phospho-threonine-320-PP1α (P-T320-PP1; Cell Signaling Technology, Cat# 2581, RRID: AB_330823), rabbit anti-phospho-tyrosine-15-cdc2 (P-Y15-cdc2; Boster Bio, Cat# P00209), rabbit anti-phospho-tyrosine-15-cdc2 (P-Y15-cdc2; Cell Signaling Technology, Cat# 4539, RRID: AB_560953), mouse anti-PP1γ (Santa Cruz Biotechnology, Cat# sc-515943), mouse anti-turboGFP, Clone 2H8 (OriGene, Cat# TA150041, RRID: AB_2622256), rabbit anti-Wee1 (Cat# 13084, RRID: AB_2713924).

Antibody-conjugated beads used in this study: mouse anti-cyclin B1 agarose (Santa Cruz Biotechnology, Cat# sc245AC, RRID: AB_627338), mouse anti-turboGFP agarose, clone 2H8 (OriGene, Cat# TA183081, RRID: AB_2622344), protein A/G PLUS-agarose (Santa Cruz Biotechnology, Cat# sc-2003, RRID: AB_10201400), mouse anti-γ-tubulin agarose conjugate (Santa Cruz Biotechnology, Cat# sc-17788AC, RRID: AB_628418), normal mouse IgG-AC (Santa Cruz Biotechnology, Cat# sc-2343, RRID: AB_737178).

Immunoprecipitation

For immunoprecipitations from soluble and pellet fractions, samples were diluted in lysis buffer (LB; 80 mM β-glycerophosphate, 15 mM $MgCl_2$, 20 mM EGTA, 20 mM Hepes pH 7.4, 100 mM NaCl, 0.1 % Igepal; Sigma-Aldrich) supplemented with a phosphatase inhibitor cocktail (PhosSTOP; Roche) and incubated with antibody and protein A/G PLUS-agarose beads or with agarose bead-conjugated antibody overnight at 4°C in constant rotation. Beads were washed twice in LB and proteins were eluted by boiling in SDS loading buffer (Laemmli sample buffer; BioRad). For total cell lysates, 5 x 10^6 cells were lysed in 180 μL high salt lysis buffer (HSB; 16 mM β-glycerophosphate, 3 mM $MgCl_2$, 4 mM EGTA, 0,5 mM DTT, 20 mM Hepes, 0.2 % Igepal, 250 mM NaCl; Sigma-Aldrich) supplemented with a phosphatase inhibitor cocktail (PhosSTOP; Roche). After 30 min incubation on ice, lysates were spun at 13.200 rpm for 10 min at 4°C (Eppendorf centrifuge 5424 R). Cleared lysates were incubated with antibody and protein A/G PLUS-agarose beads or with agarose bead-conjugated antibody overnight at 4°C in constant rotation. Beads were washed twice in LB and either proteins were eluted by boiling in SDS loading buffer (Laemmli sample buffer; BioRad) for immunoblotting analysis or further processed as described below.

Phosphorylation and dephosphorylation assays

For kinase reactions, Ips were washed twice in LB, once in kinase reaction buffer (KRB; 80 mM β-glycerophosphate, 15 mM $MgCl_2$, 20 mM EGTA, 20 mM Hepes pH 7.4, 100 μM ATP; Sigma-Aldrich) and incubated for 20 min at 37°C in KRB -/+ recombinant active Cdk1 (0.05 mg/mL; Sigma-Aldrich) and + active Cdk1 + RO-3306 (10 μM; Calbiochem). For phosphatase reactions, Ips were washed twice in LB, once in phosphatase reaction buffer (PRB; 20 mM Hepes pH 7.4, 150 mM NaCl, 1 mM DTT, 1 mM $MnCl_2$; Sigma-Aldrich) and incubated in PRB -/+ 0.01 mg/mL recombinant human PP1α (Novus Biologicals) for 20 min at 30°C.

Immunoblotting

Immunoblotting was performed as described (Serpico et al., 2019). Briefly, samples were prepared by adding SDS loading buffer (Laemmli sample buffer; BioRad) to lysates. Samples were boiled for 10 min at 99°C before being separated on SDS-PAGE (polyacrylamide percentage spanning from 6 to 12%). Proteins were blotted onto nitrocellulose membrane (GE Healthcare) using a wet-transfer system (ThermoFisher). Membranes were incubated with 5% not fat dry milk (NFDM; BioRad) or 3% bovine serum albumin (BSA; Sigma-Aldrich) in PBS or TBS (tris buffered saline; Sigma-Aldrich) supplemented with 0.01% Tween20 (Sigma-Aldrich; TPBS or TTBS, respectively) for 1 hour at rt. Then, membranes were incubated with primary antibodies, diluted in TPBS or TTBS, at 4°C overnight. After washing twice with TPBS or TTBS, filters were incubated with secondary peroxidase-conjugated antibodies, diluted in TPBS or TTBS, for 1 hour at rt. Detection was performed using an Enhanced ChemiLuminescence (ECL) kit (GE Healthcare Life Sciences). Blots were acquired using Canon CanoScan LiDE 300 scanner (Canon) and scanned at 300 dpi.

Immunofluorescence fixation and staining

Cells were either grown onto poly-D-lysine (0,1 mg/mL; Sigma-Aldrich) coated glass coverslips or spun on Superfrost plus microscope slides (Thermo-Fisher) through Shandon Cytospin centrifuge (ThermoScientific Cytospin4 Cytocentrifuge; Thermo-Fisher). After brief wash in PBS, cells were fixed with 4% paraformaldehyde (Sigma-Aldrich) in PBS (Euroclone) for 10 min at rt and then with methanol (99.9%; Exacta + Optech) at −20°C for 10 min. Cells were washed twice with PBS and permeabilized with 0,25 % Triton X-100 (Sigma-Aldrich) in PBS for 15 min (HeLa cells) or with 0,5 % Triton X-100 (Sigma-Aldrich) in PBS for 30 min (hTERT-RPE1 cells); then, cells were washed once with PBS and incubated with 3% bovine serum albumin (BSA; Sigma-Aldrich) in PBS for 1 hour at rt. Coverslips were transferred into a humidity chamber and incubated with primary antibodies in 1,5 % (w/v) BSA-PBS solution for 2 hours (for anti-α-tubulin; anti-CREST; anti-ch-Tog; anti-γ-tubulin; anti-Map4) or for 4 hours (for anti-cdc2) or overnight (for anti-P-Y15-cdc2) at 4°C. After incubation, cells were washed three times with PBS and incubated with fluorescently labelled secondary antibodies, diluted in 1,5 % BSA-PBS solution, for 1 hour at rt. DNA was stained with Hoechst 33258 (1 μg/mL; Invitrogen) by incubation for 10 min. Finally, cells were washed four times with PBS and slides mounted with Mowiol 40-88 (Sigma-Aldrich).

Microscopy

Fixed cells were imaged using an inverted confocal fluorescence microscope LSM 980 (Zeiss) equipped with a 63X/1.4 oil objective (Zeiss). Representative images were obtained collecting 3 Z-stack series over 42 μm. The acquisitions were deconvoluted and projected into one plane using the ZEN3.1 software.

QUANTIFICATION AND STATISTICAL ANALYSIS

Statistical analysis

Statistical details of the experiments, including the value of n (where n represents the number of metaphases scored), can be found in the figure legends. All data processing and statistical analysis were performed in Excel (Microsoft). Graphs were made using Excel (Microsoft).

Reproducibility

Experiments analyzed by immunoblotting and immunofluorescence were repeated 2 to 8 times with similar results.

Image analysis and quantification

Image processing, analysis, and quantifications were performed using ImageJ software.

Analysis of chromosome alignment

For quantitative analyses of immunofluorescence experiments investigators were blinded to sample allocation. Metaphases were visually scored and those with more than three chromosomes falling outside the two internal quarters of the interpolar distance were considered misaligned; around 100 cells were scored in 4 fields of each slide for each experimental condition.

Cell Reports, Volume *38*

Supplemental information

Compartmentalized control of Cdk1 drives mitotic spindle assembly

Angela Flavia Serpico, Francesco Febbraro, Caterina Pisauro, and Domenico Grieco

Supplemental information

Supplemental Figures

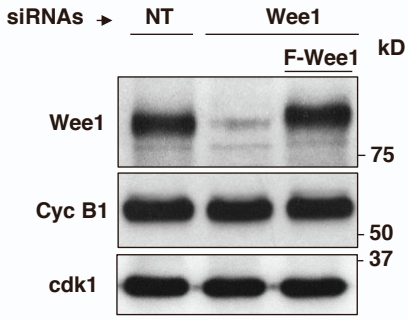

Figure S1. siRNA treatment of hTERT-RPE1 cells, Related to Figure 1.

Lysates of hTERT-RPE1 cells treated with non-targeting siRNAs (NT) and with Wee1-siRNAs (Wee1) as described in Figure 1 were probed for indicated antigens. A portion of Wee1-siRNA-treated cells was previously transfected with a siRNA-resistant, 3XFlag-tagged Wee1 expression vector (F-Wee1).

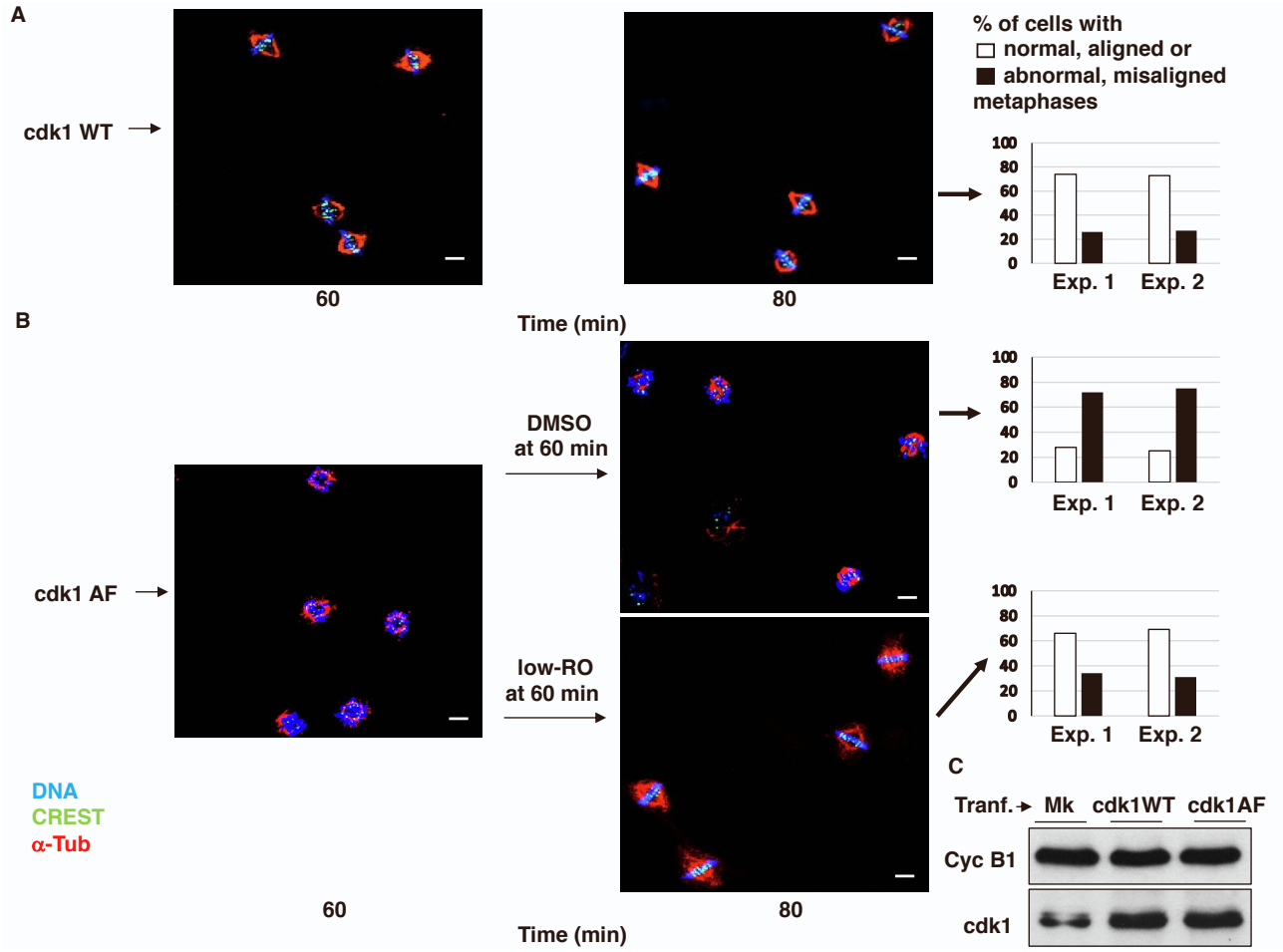

Figure S2. Expression of an inhibitory phosphorylation-resistant version of Cdk1 impairs spindle assembly, Related to Figure 1.

hTERT-RPE1 cells were transfected with (A) wild type cdk1 (cdk1WT) expression vector or (B) a mutant cdk1 expression vector in which cdk1-threonine 14 and tyrosine 15 are mutated into non-phosphorylatable alanine and phenylalanine, respectively (cdk1AF). 6 hours post transfection, cells were arrested at G2 by addition of high-RO for further 16 hours incubation. Cells were fixed and stained for DNA (blue), α-tubulin (red) and CREST (green) at 60 and 80 min upon release from G2 arrest. A portion of cdk1AF-transfected cells received low-RO at 60 min; as control vehicle was added (DMSO). Graphs: y axis = percent of cells containing normal aligned (white bar) or abnormal misaligned (black bar) spindles at 80 min incubation; x axis = data from two independent experiments (Exp. 1; Exp. 2); around 100 cells were scored in 4 independent microscopy slide fields. Scale bar: 5 μm. (C) samples of cells treated as in (A) and (B) were lysed prior to release and probed for indicated antigens.

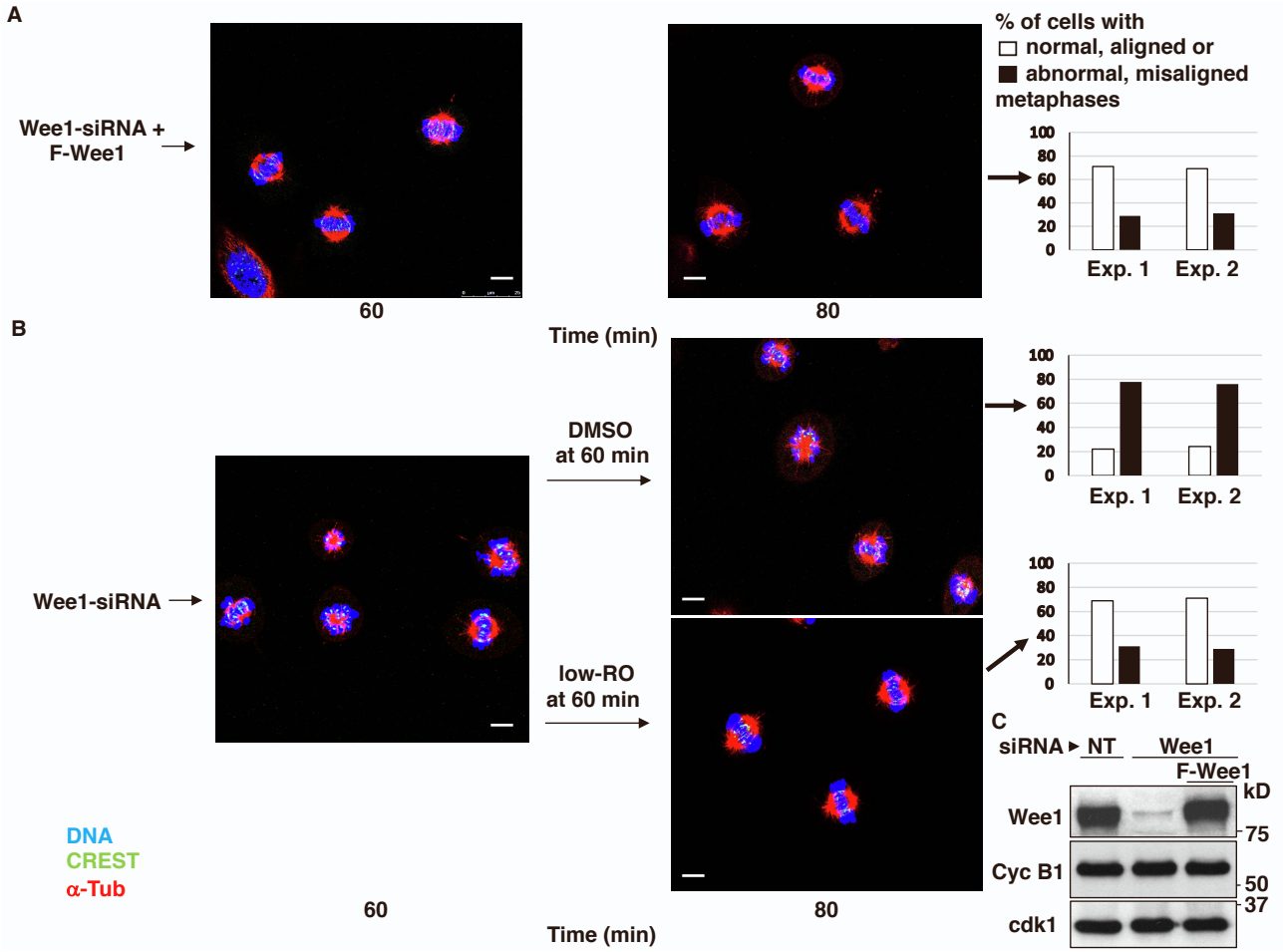

Figure S3. Downregulation of Wee1 impairs spindle assembly in HeLa cells, Related to Figure 1.

HeLa cells were treated and arrested at G2 as described for hTERT-RPE1 cells in Figure 1A. Cells were fixed and stained for DNA (blue), α-tubulin (α-Tub; red) and CREST (green) at 60 and 80 min upon release from G2 arrest. (A) Wee1-siRNA-treated cells complemented with siRNA-resistant expression vector (Wee1-siRNAs + F-Wee1). (B) Wee1-siRNA-treated cells (Wee1-siRNAs). A portion of Wee1-siRNAs cells received low-RO at 60 min; as control vehicle was added (DMSO). Graphs: y axis = percent of cells containing normal aligned (white bar) or abnormal misaligned (black bar) spindles at 80 min incubation; x axis = data from two independent experiments (Exp. 1; Exp. 2); around 100 cells were scored in 4 independent microscopy slide fields. Scale bar: 5 μm. C, samples of cells treated as in (A) and (B) were lysed prior to release and probed for indicated antigens.

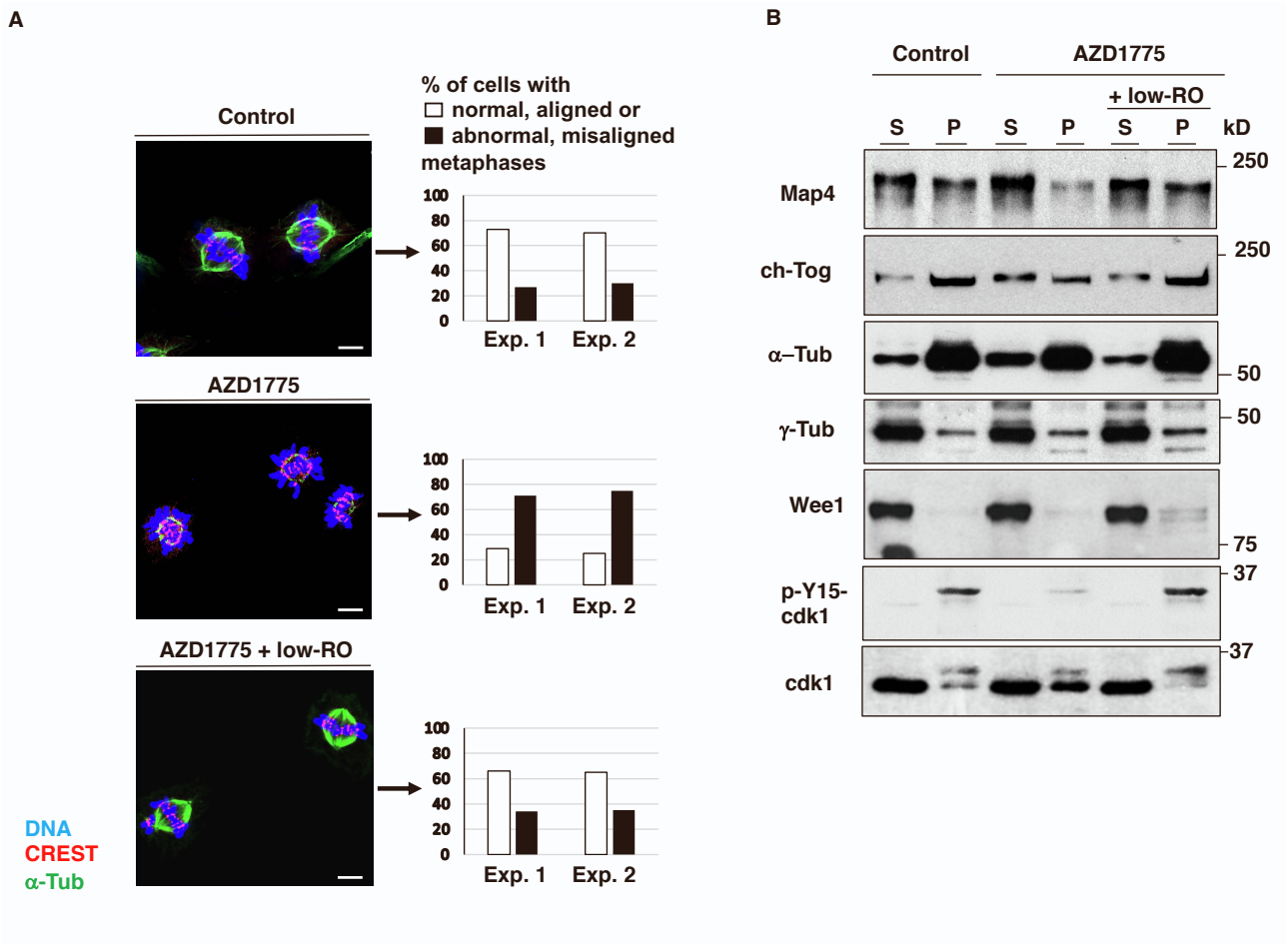

Figure S4. Chemical inhibition of Wee1 impairs spindle assembly and Wee1 downregulation delays mitosis exit, Related to Figure 1.

(A) hTERT-RPE1 cells were released from a G2 arrest by high-RO treatment into M/C medium and either vehicle (Control) or AZD1775 was added. Cells were fixed after further 80 min of incubation and stained for α-tubulin (α-Tub, green), centromeres (red) and DNA (blue). A sample of the AZD1775-treated cells also received low-RO 60 min post release. Graphs: y axis = percent of cells containing normal aligned (white bar) or abnormal misaligned (black bar) spindles at 80 min incubation; x axis = data from two independent experiments (Exp. 1; Exp. 2); around 100 cells were

scored in 4 independent microscopy slide fields. Scale bar: 5 μm. (B) prometaphase-arrested hTERT-RPE1 were released into M/C medium and either vehicle (Control) or AZD1775 was added. S and P fraction were prepared after further 80 min of incubation and probed for indicated antigens. A sample of the AZD1775-treated cells also received low-RO 60 min post release. (C) Non-targeting-siRNA- (Control) or Wee1-siRNA-treated (Wee1) hTERT-RPE1 cells were arrested at prometaphase and released into fresh medium for 60 min of incubation. Cells were lysed and probed for indicated antigens.

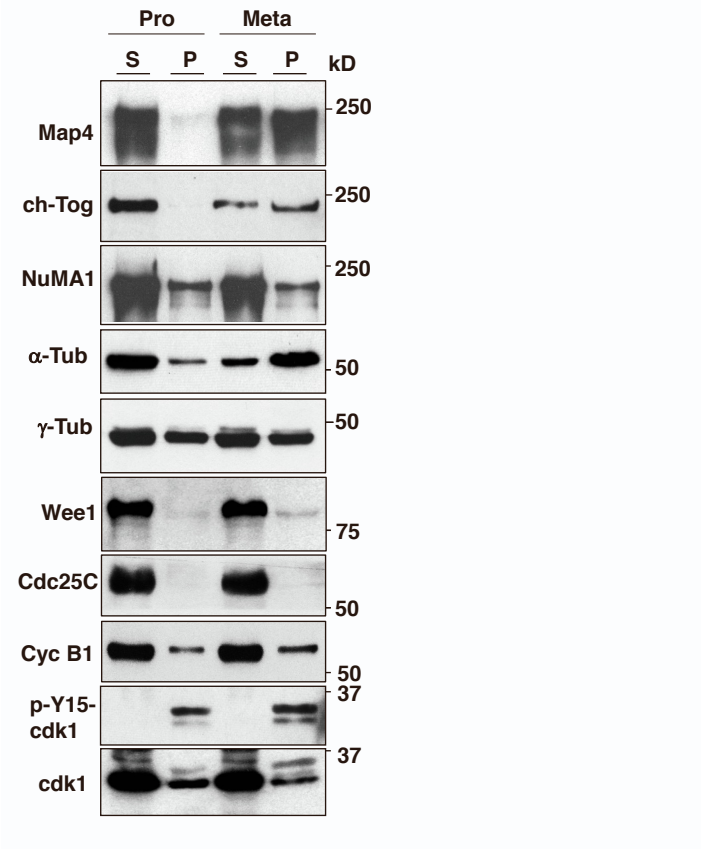

Figure S5. Mitotic HeLa cell fractionation, Related to Figure 2.

Prometaphase-arrested HeLa cells were collected and taken immediately (Pro) or released in M/C medium for 60 min (Meta). Fractionated S and P fractions were probed for indicated antigens (P fraction enriched 4 folds over S fraction; see Methods).

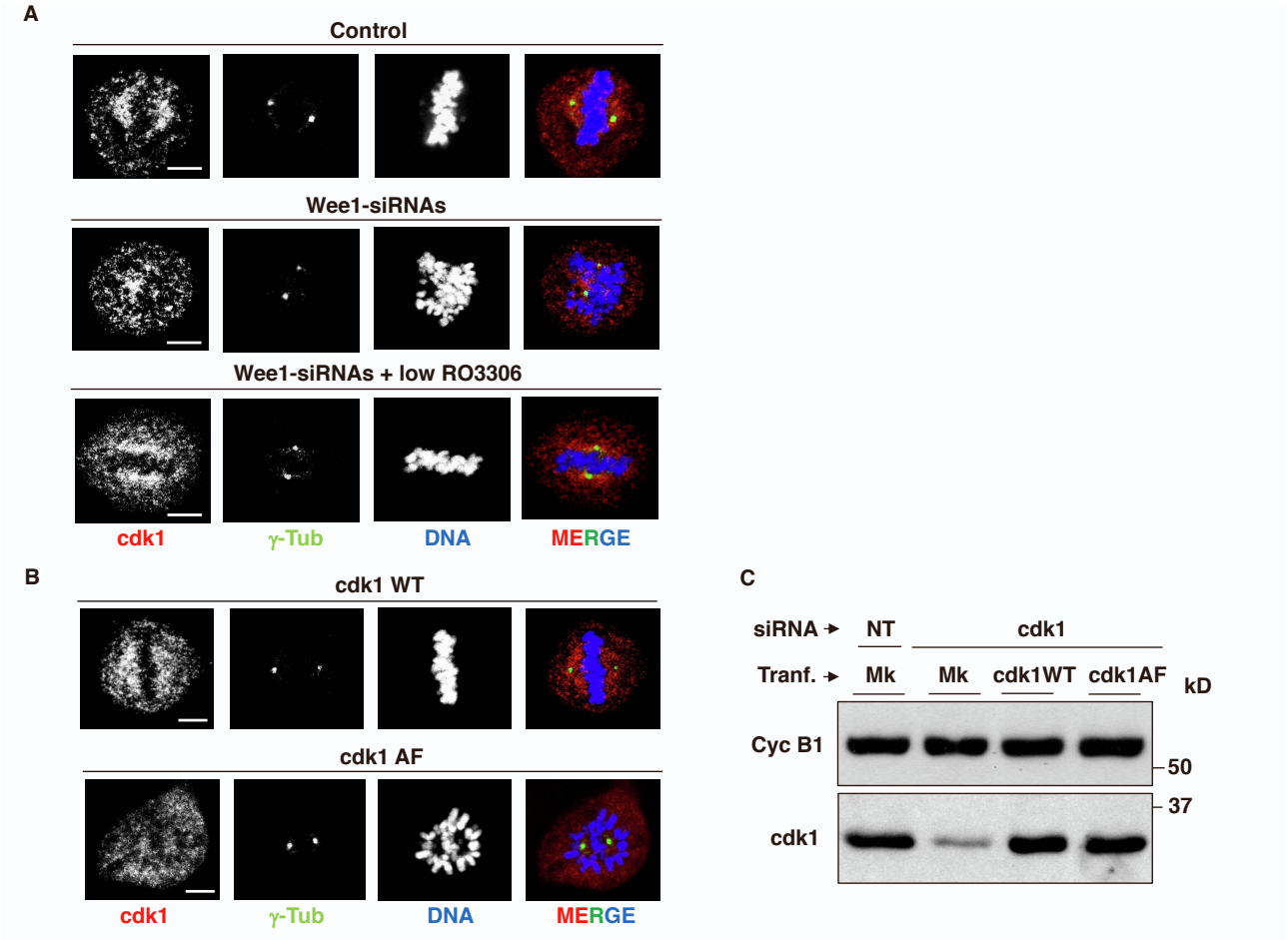

Figure S6. Cdk1 localization in Wee1-siRNA-treated HeLa cells and cdk1AF expressing hTERT-RPE1 cells, Related to Figure 2.

(A) HeLa cells were treated with non-targeting-siRNAs (Control) and Wee1-siRNAs, prometaphase-arrested and released in M/C medium for 80 min incubation as described in Figure 1B and a portion of Wee1-siRNA-treated cells received low-RO at 60 min post release (efficiency of Wee1 downregulation was similar to that shown in Figure S1). Cells were fixed and stained for indicated antigens. (B, C) hTERT-RPE1 cells were treated with cdk1-siRNAs and transfected with siRNA-resistant cdk1WT or cdk1AF expression vectors after 12 hours. Then arrested at prometaphase by a 16-hour treatment with nocodazole, released and fixed after 80 min of incubation in M/C medium. Cells were fixed and stained for indicated antigens. Scale bar: 5 μm. (C) hTERT-RPE1 cells treated with non-targeting (NT), cdk1-trageting siRNAs and cdk1-siRNAs plus transfection (Tranf.) with siRNA-resistant cdk1WT or cdk1AF for the same duration as in (B) were lysed and probed for the indicated antigens (mock transfection: Mk).

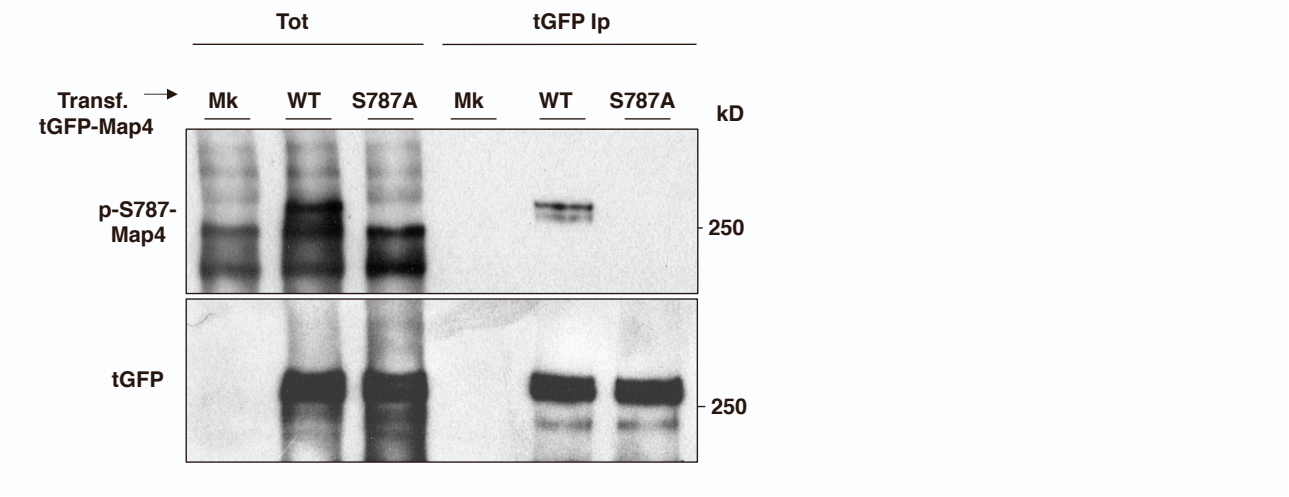

Figure S7. Detection of S787-Map4 phosphorylation, Related to Figure 3.

hTERT-RPE1 cells were transfected with expression vectors of tGFP-Map4 wild type (WT) or tGFP-Map4 mutant version in which serine 787 of Map4 was mutated into alanine (S787A) and arrested at prometaphase. Total cell lysates (Tot) and relative anti-tGFP Ips were probed for indicated antigens (Mk: mock transfection).

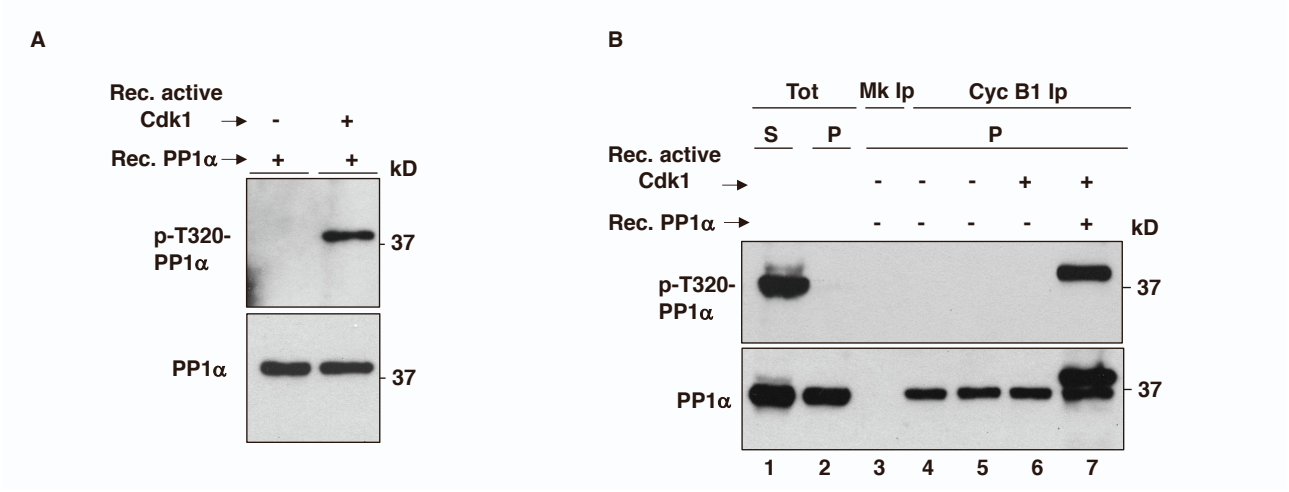

Figure S8. i-Cdk1-bound PP1α resists to phosphorylation by active Cdk1 in vitro, Related to Figure 4.

(A) Recombinant PP1α (+ Rec. PP1α) was incubated in kinase reaction buffer at 37° C for 15 min in the absence (-) or presence (+) of recombinant, active, Cdk1 (+ Rec. active Cdk1). Reactions were then probed for indicated antigens. (B) Lanes 1, 2: total S and P fractions of metaphase hTERT-RPE1 cells; lane 3: mock Ips from P fraction; lanes 4-7: cdk1 Ips from P fractions; lane 4: Ips were immediately mixed with loading buffer; lane 5-7: Ips were incubated in kinase reaction buffer at 37° C for 15 min in the absence (lane 5) or presence (lane 6) of recombinant, active, Cdk1 (+ Rec. active Cdk1) and (lane 7) with recombinant, active, Cdk1 and recombinant PP1α (+ Rec. active Cdk1, + Rec. PP1α). Samples were, then, probed for indicated antigens.